Impact of reactive surfaces on the abiotic reaction between nitrite and ferrous iron and associated nitrogen and oxygen isotope dynamics

Anna-Neva Visser[1,4], Scott D. Wankel[2], Pascal A. Niklaus[3], James M. Byrne[4], Andreas A. Kappler[4], Moritz F. Lehmann[1]

[1]Department of Environmental Sciences, Basel University, Bernoullistrasse 30, 4056 Basel, Switzerland
[2]Woods Hole Oceanographic Institution, Woods Hole, 360 Woods Hole Rd, MA 02543, USA
[3]Department of Evolutionary Biology and Environmental Studies, University of Zürich, Winterthurerstrasse 190, 8057 Zürich, Switzerland
[4]Department of Geosciences, Tübingen University, Hölderlinstrasse 12, 72074 Tübingen, Germany

Correspondence to: Anna-Neva Visser (a.visser@unibas.ch)

Abstract. Anaerobic nitrate-dependent Fe(II) oxidation (NDFeO) is widespread in various aquatic environments, and plays a major role in iron and nitrogen redox dynamics. However, evidence for truly enzymatic, autotrophic NDFeO remains limited, with alternative explanations involving coupling of heterotrophic denitrification with abiotic oxidation of structurally-bound or aqueous Fe(II) by reactive intermediate N species (chemodenitrification). The extent to which chemodenitrification is caused, or enhanced, by *ex vivo* surface catalytic effects has, so far, not been directly tested. To determine whether the presence of either a Fe(II)-bearing mineral or dead biomass (DB) catalyses chemodenitrification, two different sets of anoxic batch experiments were conducted: 2 mM Fe(II) was added to a low-phosphate medium, resulting in the precipitation of vivianite ($Fe_3(PO_4)_2$), to which later 2 mM nitrite (NO_2^-) was added, with or without an autoclaved cell suspension (~1.96×10^8 cells ml^{-1}) of *Shewanella oneidensis* MR-1. Concentrations of nitrite, nitrous oxide (N_2O) and iron (Fe^{2+}, Fe_{tot}) were monitored over time in both setups to assess the impact of Fe(II) minerals and/or DB as catalysts of chemodenitrification. In addition, the natural-abundance isotope ratios of NO_2^- and N_2O ($\delta^{15}N$ and $\delta^{18}O$) were analysed to constrain associated isotope effects. Up to 90% of the Fe(II) was oxidized in the presence of DB, while only ~65% were oxidized under mineral-only conditions, suggesting an overall lower reactivity of the mineral-only setup. Similarly, the average NO_2^- reduction rate in the mineral-only experiments (0.004 ±0.003 mmol L^{-1} day^{-1}) was much lower compared to experiments with mineral plus DB (0.053 ±0.013 mmol L^{-1} day^{-1}), as was N_2O production (204.02 ±60.29 nmol/L*day). The N_2O yield per mole NO_2^- reduced was higher in the mineral-only setups (4%) compared to the experiments with DB (1%), suggesting the catalysis-dependent differential formation of NO. N-NO_2^- isotope ratio measurements indicated a clear difference between both experimental conditions: In contrast to the marked ^{15}N isotope enrichment during active NO_2^- reduction ($^{15}\varepsilon_{NO2} = +10.3‰$) observed in the presence of DB, NO_2^- loss in the mineral-only experiments exhibited only a small N isotope effect (<+1‰). The NO_2^--O isotope effect was very low in both setups ($^{18}\varepsilon_{NO2}$<1‰), most likely due to substantial O isotope exchange with ambient water. Moreover, during the low-turnover conditions (i.e. in the mineral-only experiments, as well as initially in experiments with DB), the observed NO_2^- isotope systematics suggest, transiently, a small inverse isotope effect (i.e. decreasing NO_2^- $\delta^{15}N$ and $\delta^{18}O$ with decreasing

concentrations), possibly related to transitory surface complexation mechanisms. Site preference (SP) of the ^{15}N isotopes in the linear N_2O molecule for both setups ranged between 0 to 14‰, notably lower than previously reported for chemodenitrification. Our results imply that chemodenitrification is dependent on the available reactive surfaces, and that the NO_2^- (rather than the N_2O) isotope signatures may be useful for distinguishing between chemodenitrification catalysed by minerals, chemodenitrification catalysed by dead microbial biomass, and possibly true enzymatic NDFeO.

1. Introduction

Iron (Fe) is essential for all living beings and its biogeochemical cycling has been studied extensively (Expert, 2012; Lovley, 1997). Although Fe is ubiquitous in most environments, it is not always bioavailable (Andrews et al., 2003; Ilbert and Bonnefoy, 2013), and microorganisms must often cope with Fe limitation in their respective environments (Braun and Hantke, 2013; Ilbert and Bonnefoy, 2013). This is especially true at circumneutral pH and oxic conditions, where Fe(II) is quickly oxidized by O_2 and thus only present as poorly soluble Fe(III)(oxyhydr)oxides (Cornell and Schwertmann, 2003; Stumm and Sulzberger, 1992). In contrast, under anoxic conditions, Fe is mainly present as either dissolved Fe^{2+} or as mineral-bound Fe(II) in Fe phosphates or carbonates (Charlet et al., 1990; Luna-Zaragoza et al., 2009). Here, microbes use electron acceptors other than O_2 for respiration (He et al., 2016; Lovley, 2012; Straub et al., 1996). One redox pair that has been proposed to be exploited by microbes under anoxic conditions is NO_3^-/Fe^{2+}, through a mechanism known as nitrate-dependent Fe(II) oxidation (NDFeO) (Ilbert and Bonnefoy, 2013; Straub et al., 1996). To date, genetic evidence that clearly supports this metabolic capacity of the studied microorganisms remains lacking (Price et al., 2018), and biogeochemical evidence is rare and putative. The latter is mostly based on experiments with the chemolithoautotrophic culture KS, a consortium of four different strains, including a relative of the microaerophilic *Sideroxydans*/*Gallionella*. This enrichment culture has been shown to be able to oxidize Fe(II) without the addition of any organic co-substrates (Tominski et al., 2018). Tian et al. (2020) confirmed that *Gallionellaceae* are able to perform autotrophic Fe(II)-dependent denitrification. Another more indirect line of evidence includes results from slurry microcosm experiments with marine coastal sediments. In these experiments, Fe(II) oxidation was still detected even after all bioavailable organics of the sediments were consumed and only NO_3^- was left (Laufer et al., 2016). With regards to other studies where NDFeO was initially thought to be performed by autotrophs (Chakraborty et al., 2011; Weber et al., 2009), it was subsequently shown that the microbes rely on an organic co-substrate and must in fact be considered mixotrophic (Klueglein et al., 2014; Muehe et al., 2009). Yet, the exact mechanism promoting NDFeO in the microorganisms that have been investigated so far (e.g. *Acidovorax delafieldii* strain 2AN, *Pseudogulbenkiania ferrooxidans* strain 2002) (Chakraborty et al., 2011; Weber et al., 2009), is still not fully understood. It has been suggested that extracellular electron transfer (EET) might play a major role in NDFeO, particularly in the presence of high levels of extracellular polymeric substances (EPS) (Klueglein et al., 2014; Liu et al., 2018; Zeitvogel et al., 2017). EPS has been demonstrated to act as electron shuttles, hence EET may indeed provide a plausible explanation for the observed Fe(II) oxidation in these cultures (Liu et al., 2018). The existence of such an electron transfer would imply that NDFeO is not necessarily a completely enzymatically-catalysed

reaction. Considering that all putative NDFeO strains were grown under high (up to 10 mM) nitrate (NO_3^-) and Fe(II) concentrations, and accumulated up to several mM nitrite (NO_2^-) from enzymatic NO_3^- reduction, other studies suggested that the observed Fe(II) oxidation in these pure cultures may be due to the abiotic side reaction between the generated NO_2^- and Fe(II) (Buchwald et al., 2016; Prakash Dhakal, 2013; Klueglein et al., 2014). This abiotic reaction between NO_2^- and Fe(II) is known as chemodenitrification (Equation 1) and is proposed to lead to an enhanced production of N_2O (Anderson and Levine, 1986; Buchwald et al., 2016; Zhu-Barker et al., 2015).

$$4Fe^{2+} + 2NO_2^- + 5H_2O \rightarrow 4FeOOH + N_2O + 6H^+ \qquad \Delta G^\circ = -128.5\ {}^{kJ}/_{mol} \qquad (1)$$

Several studies have noted that the presence of reactive surfaces may enhance the abiotic reaction (Heil et al., 2016; Sorensen and Thorling, 1991). For example, Klueglein and Kappler (2013) tested the impact of goethite on Fe-coupled chemodenitrification in the presence of high Fe(II) and NO_2^- concentrations, and confirmed the concentration dependency of this reaction with regard to both species (Van Cleemput and Samater, 1995). Possible catalytic effects (e.g. by reactive surfaces and/or organic matter) were not tested specifically in these studies. Yet, multiple factors have been shown to affect the abiotic reaction between NO_2^- and Fe(II) and may need to be considered (i.e. pH, temperature, Fe^{2+} concentrations, solubility of Fe(III)(oxyhydr)oxides, crystallinity of Fe(II) minerals, other metal ion concentrations and catalytic effects) (Van Cleemput & Samater, 1995; Klueglein & Kappler, 2013; Ottley et al., 1997). In addition, the presence of organic compounds can lead to the abiotic reduction of NO_2^- to NO (Van Cleemput and Samater, 1995; McKnight et al., 1997; Pereira et al., 2013).

Given the complex controls and potential interaction between Fe(II) and various nitrogenous compounds, including intermediates, it may be an oversimplification to state that Fe(II) oxidation observed in previous laboratory setups is solely caused by the abiotic reaction with NO_2^-, and not, for example, stimulated by reactive surfaces (minerals, organic-detritus) or by nitric oxide (NO), a highly reactive intermediate not easily quantified in anoxic experiments. In order to better understand the factors that may control chemodenitrification of NO_2^-, this study focuses on the possible catalytic surface effects induced by a Fe(II) mineral phase or dead biomass (DB). Furthermore, microbial cells, DB, or detrital waste products might not only provide additional reactive surface area, but may directly react with NO_2^- to form NO.

Stable isotopes of both N and O ($\delta^{15}N$ and $\delta^{18}O$) offer a promising approach to further elucidate the mechanism of NDFeO, and also to more generally expand our understanding of chemodenitrification. The N and O isotopic composition of nitrogenous compounds (e.g. NO_3^-, NO_2^-, and N_2O) has been used to gain deeper insights into various N turnover processes (Granger et al., 2008; Jones et al., 2015). The dual NO_2^- (or NO_3^-) isotope approach is based on the fact that specific N-transformation processes – biotic or abiotic – are associated with specific N and O isotope fractionation (i.e. isotope effect). In general, enzymatic processes promote the more rapid reaction of lighter N and O isotopologues, leaving the remaining substrate pool enriched in the heavier isotopes (i.e. ^{15}N, ^{18}O) (Granger et al., 2008; Kendall & Aravena, 2000; Martin & Casciotti, 2017). Only a few studies exist that have looked into the isotope effects of chemodenitrification and reports on the associated isotope effects are variable. Consistent with what we know from biological denitrification, chemodenitrification experiments with 10 mM Fe(II) and NO_2^-, with very high reaction rates, revealed a significant increase in the $\delta^{15}N$ (up to 40‰) and $\delta^{18}O$ (up to

30‰) NO_2^- values, corresponding to an overall N and O isotope effect of $^{15}\varepsilon$ 18.1 ± 1.7‰ and $^{18}\varepsilon$ 9.8 ± 1.8‰, as well as a $\Delta^{15}N$ (i.e. the difference between $\delta^{15}NO_2^-$ and $\delta^{15}N_2O$) of 27 ± 4.5‰ (Jones et al., 2015). However, reaction kinetics can significantly affect isotope reaction dynamics, and chemodenitrification is possibly impacted by e.g. concentration effects and/or the presence of different catalysts (i.e. surfaces, organics). Hence, performing coupled N and O isotope measurements might help to gain deeper insights into the mechanistic details and fractionation systematics of NO_2^- reduction in the presence of Fe(II). Here, in order to expand the limited dataset on the isotope effects of abiotic Fe(II)-coupled denitrification, and in turn to lay the groundwork for using NO_3^-/NO_2^- N and O isotope measurements to unravel the mechanism behind NDFeO, we studied the N and O isotope dynamics of NO_2^- reduction and N_2O production during abiotic reaction of NO_2^- with Fe(II). As the extent of the formation of various Fe(III)(oxyhydr)oxides has been previously reported to enhance chemodenitrification dynamics (Chen et al., 2018; Sorensen and Thorling, 1991), we also followed mineral alteration during chemodenitrification in order to identify possible reaction patterns. A specific goal in this context was to assess the impact of Fe(II) precipitates and/or dead biomass as catalytic agents during Fe(II)-associated chemodenitrification, as well as potential mineral transformation processes associated with the abiotic oxidation of Fe(II) via reactive NO_x species.

2. Material and Methods

2.1. General experimental setup

For all experiments, anoxic low phosphate medium (1.03 mM KH_2PO_4, 3.42 mM NaCl, 5.61 mM NH_4Cl, 2.03 mM $MgSO_4 \cdot 7 H_2O$ and 0.68 mM $CaCl_2 \cdot 2 H_2O$, with a 7-vitamin (Widdel & Pfennig, 1981) and a SL-10 trace element solution (Widdel et al., 1983); 22 mM bicarbonate buffered) was prepared. The medium was dispensed with a Widdel flask in 1-l Schott bottles and the pH for each bottle was adjusted separately by the addition of anoxic, sterile 1 M HCl. For both setups, five different pH values were targeted: 5.8, 6.2, 6.5, 6.9 and 7.1. After pH adjustment, $Fe(II)Cl_2$ was added to reach a concentration of ~2 mM Fe(II), and, if necessary, the pH was re-adjusted. The medium was kept for 48 h at 4°C, resulting in amorphous, green-greyish Fe(II) precipitates. In addition, ~2 mM $NaNO_2$ and ~1 mM Na-acetate were added to the main medium stocks shortly before 10 ml aliquots of the medium were distributed into 20 ml headspace vials (heat-sterilized) in an anoxic glove box (MBraun, N_2, 100%). Acetate was added to mimic experiments, in which bacteria are cultivated (yet, acetate concentrations did not change during incubations, underscoring that the organic acid was not involved in the observed reactions; data not shown). All headspace vials were closed with black butyl stoppers and crimp-sealed [headspace N_2/CO_2 (90/10, v/v)]. All vials were then incubated at 28°C in the dark.

Incubations with dead-biomass – *Shewanella oneidensis* MR-1, a facultative aerobic Gram-negative bacterium, is seen as model organism for bioremediation studies due to its various respiratory abilities (Heidelberg et al., 2002; Lies et al., 2005). It is known to perform dissimilatory metal reduction by utilizing alternative terminal electron acceptors such as elemental sulfur, Mn(IV), Fe(III) or NO_3^-. Since *S. oneidensis* produces large amounts of EPS (Dai et al., 2016; Heidelberg et al., 2002), but is not capable of oxidizing Fe(II) (Lies et al., 2005; Piepenbrock et al., 2011) (i.e. no interference with abiotic reactions involving

Fe/chemodenitrification), we chose concentrated and sterilized *S. oneidensis* for our dead-biomass experiments. In preparation of these experiments, *S. oneidensis* MR-1 was grown oxically on a LB (lysogeny broth) medium (10 g tryptone, 5 g yeast extract, 10 g NaCl in 1 l DI water) in six 250 ml Erlenmeyer flasks. After 12 hrs, cultures were transferred into 50 ml Falcon tubes and centrifuged for 25 min at 4000 rpm (Eppendorf, 5430 R). Cell-containing pellets were washed twice with oxalic acid and centrifuged again, followed by three more washing steps with TRIS buffer prior to final resuspension in 5 ml TRIS buffer. Pellet suspensions were pooled in a 100 ml serum bottle and autoclaved twice to ensure that all cells were killed. Before distribution of the medium into 20 ml vials (see above), cell suspension was added to yield a cell density of ~1.96×10^8 cell ml^{-1}. Care was taken to ensure the homogenous distribution of mineral precipitates and the dead biomass.

2.2. Sampling and sample preparation

Incubations were run for approximately 30 days, and sampling was performed in an anoxic glove box (MBraun, N_2, 100%) at five time points. For each time point, and for each pH treatment, 9 replicates were prepared. Therefore, variations between the replicates and the different sampling time points are possible. For sampling, the headspace was quantitatively transferred into 12 ml He-purged Exetainer vials (LABCO) for N_2O concentration measurements. Then, 2 ml of the liquid sample were transferred into 2 ml Eppendorf tubes, centrifuged for 5 min (13400 rpm; Eppendorf, MiniSpin), followed by a 1:10 dilution of the supernatant in 1 ml anoxic MilliQ water for NO_2^- quantification. A second 100 µl aliquot was diluted 1:10 in 40 mM sulfamic acid (SFA) for iron determination by ferrozine analysis (Granger and Sigman, 2009; Klueglein and Kappler, 2013). The remaining supernatant was used for HPLC and NO_2^- isotope analysis. Finally, the spun-down pellet was resuspended in 1 M HCl for ferrozine analysis (Stookey, 1970). All liquid samples were stored at 4°C in the dark until further processing. The remaining liquid samples were used for ^{57}Fe Mössbauer spectroscopy.

2.3. Analytical techniques

NO_2^- concentrations – NO_2^- concentrations were quantified within one hour after the sample was taken via a standard segmented continuous-flow analytical (CFA, SEAL Analytics) photometric technique (Snyder and Adler, 1976). NO_2^- reduction rates were calculated based on the observed net concentration decrease ($\overline{[C]}_{t0} - \overline{[C]}_{tend}$ ±standard error) with time.

Fe concentrations – SFA- and/or HCl-fixed samples were stored in the dark and at 4°C until Fe(II) concentrations were analysed using the ferrozine assay (Stookey, 1970), which was adapted for NO_2^--containing samples by Klueglein et al. (2013). Total Fe(II) concentrations were calculated as the sum of the $Fe_{aq}^{2+} + Fe(II)_{pellet}$ concentrations.

N_2O concentrations – Prior to the quantification of the N_2O, the sample gas was diluted (1:5) with 5.0 He. Triplicate samples were then analysed using a gas chromatograph with an electron capture detector (GC-ECD; Agilent 7890 with micro-ECD and FID; Porapak Q 80/100 column). GC-ECD measurements were calibrated using four standard gases containing different concentrations of N_2O (Niklaus et al., 2016). N_2O production rates were calculated based on the observed net N_2O concentration increase ($\overline{[C]}_{tend} - \overline{[C]}_{t0}$ ±standard error) with time.

^{57}Fe Mössbauer spectroscopy - For Mössbauer spectroscopic analyses, the remaining liquid samples (ca. 8 ml) were processed inside an anoxic glove box. The entire liquid including the precipitates was passed through a 0.45 µm filter. The wet filter was then sealed between two layers of Kapton tape and kept inside sealed Schott bottles in a freezer (-20°C) under anoxic conditions until analysis. From the treatments with DB, samples were collected at day 0 at pH 6.8 and at the end of the experiment (~30 days) for pH 6.8 and 5.8. For the mineral-only experiment, only one sample (time point zero, pH 6.8) was analysed, as a basis for comparison with the DB experiments (i.e. to verify whether DB has an immediate effect on the mineral phase). Taking care to minimize exposure to air, samples were transferred from the air-tight Schott bottles and loaded inside a closed-cycle exchange gas cryostat (Janis cryogenics). Measurements were performed at 77 K with a constant acceleration drive system (WissEL) in transmission mode with a ^{57}Co/Rh source and calibrated against a 7µm thick α-^{57}Fe foil measured at room temperature. All spectra were analysed using Recoil (University of Ottawa) by applying a Voight Based Fitting (VBF) routine (Lagarec and Rancourt, 1997; Rancourt and Ping, 1991). The half-width at half maximum (HWHM) was fixed to a value of 0.130 mm/s during fitting.

Nitrite N and O isotope measurements – The nitrogen (N) and oxygen (O) isotope composition of NO_2^- was determined using the azide method (McIlvin and Altabet, 2005). This method is based on the chemical conversion of NO_2^- to gaseous N_2O at a low pH (4 to 4.5) (McIlvin and Altabet, 2005), and the subsequent analysis of the concentrated and purified N_2O by gas chromatography-isotope ratio mass spectrometry (GC-IRMS). Addition of 0.6 M NaCl to the acetic acid-azide solution was conducted in order to minimize oxygen isotope exchange (McIlvin and Altabet, 2005). The acetic acid-azide solution was prepared freshly every day (McIlvin and Altabet, 2005) and kept in a crimp sealed (grey butyl stopper) 50 ml serum bottle. Sample volume equivalent to 40 nmol NO_2^- was added to pre-combusted headspace vials, filled up to 3 ml with anoxic MilliQ water, and crimp-sealed. Then, 100 µl of the acetic acid/azide solution was added. After ~7 hrs, 100 µl of 6 M NaOH was added to stop the reaction. Until isotope analysis by a modified purge and trap gas bench coupled to CF-IRMS (McIlvin and Casciotti, 2010), the samples were stored upside down at room temperature and in the dark. Two nitrite isotope standards, namely N-7373 (δ^{15}N: -79.6‰, δ^{18}O: +4.5‰) and N-10219 (δ^{15}N: +2.8‰; δ^{18}O; +88.5‰)(Casciotti & McIlvin, 2007), were prepared on the day of isotope analysis and processed the same way as samples. N and O isotope data are expressed in the common δ notation and reported as permil deviation (‰) relative to AIR N_2 and VSMOW, respectively (($\delta^{15}N = ([^{15}N]/[^{14}N])_{sample} / [^{15}N]/[^{14}N]_{air\_N2} - 1) \times 1000‰$ and $\delta^{18}O = ([^{18}O]/[^{18}O]_{sample} / [^{18}O]/[^{16}O]_{VSMOW} - 1) \times 1000‰$). Based on replicate measurements of laboratory standards and samples, the analytical precision for NO_2^- δ^{15}N and δ^{18}O analyses was ±0.4‰ and ±0.6‰ (1 SD), respectively.

N_2O N and O isotope measurements – Triplicate 12 nmol samples of N_2O were injected into 20 ml headspace vials that were flushed before for 5 hrs with 5.0 He (injection volumes according to the N_2O concentrations determined before). The N_2O was then analysed directly using CF-IRMS (see above). Two standard gases with known δ^{15}N and δ^{18}O values were analysed along with the samples, namely FI.CA06261 (δ^{15}N: -35.74‰, $\delta^{15}N^{\alpha}$: -22.21‰, $\delta^{15}N^{\beta}$=-49.28‰, δ^{18}O: 26.94‰) and FI.53504 (δ^{15}N: 48.09‰, $\delta^{15}N^{\alpha}$: 1.71‰, $\delta^{15}N^{\beta}$=94.44‰, δ^{18}O: 36.01‰) (provided by J. Mohn, EMPA; e.g. Mohn et al., 2014). The gases were calibrated on the Tokyo Institute of Technology scale for bulk and site-specific isotopic composition (Ostrom et al., 2018;

Sakae Toyoda et al., 1999). Ratios of m/z 45/44, 46/44 and the 31/30 signals were used to calculate values of $\delta^{15}N^{bulk}$ (referenced against AIR-N_2), $\delta^{18}O$ (referenced against V-SMOW), and site-specific $\delta^{15}N^{\alpha}$, $\delta^{15}N^{\beta}$ based on Frame and Casciotti (2010) . Site preference (SP) was calculated as $\delta^{15}N^{\alpha} - \delta^{15}N^{\beta}$ (Sutka et al., 2006; Toyoda and Yoshida, 1999).

2.4. Pourbaix diagram

In order to predict the stability and behaviour of the N- and Fe(II)-bearing chemical species in the same system, a Pourbaix (Eh-pH) diagram was constructed (Delahay et al., 1950) as a valuable tool to predict possible reactions and speciation of end products under different experimental conditions. To calculate the enthalpies for the stepwise reduction of nitrite during denitrification, as well as Fe(II) oxidation reactions, standard enthalpy values were taken from different references (Table S1). The Pourbaix diagram presented in the discussion was devised using concentrations measured during the experiments performed for this study.

3. Results

3.1. Chemodenitrification kinetics

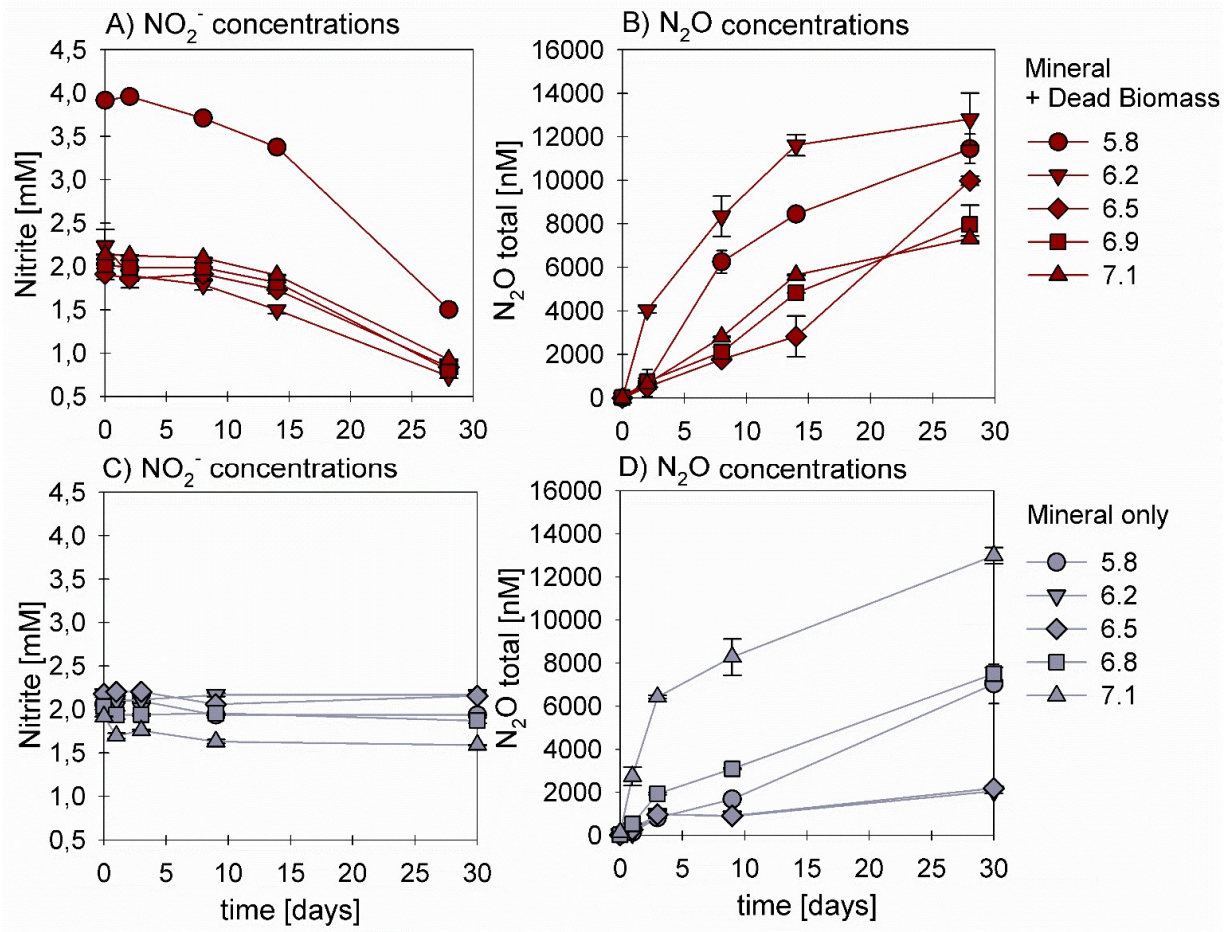

Figure 1: Nitrite reduction (A, C) and N_2O production (B, D) over time in the mineral + dead biomass (red) and mineral-only (grey) setups over time and at different pH. Please note that at pH 5.8 twice the amount of nitrite was accidently introduced. Standard error calculated from biological replicates (n = 9) is represented by the error bars.

In the presence of DB, NO_2^- reduction rates were much higher compared to the mineral-only setup (Figure 1 A, C), with up to ~60% of the initially amended NO_2^- being transformed during the incubation period, independent of the pH. The addition of DB led to a decrease in NO_2^- concentrations from 2 mM to ~0.7 mM (Figure 1 A). The pH 5.8 treatment (unintentionally amended with 2x NO_2^-) also showed a similar fractional reduction. In the mineral-only setups the decrease in NO_2^- concentration was rather moderate and ranged between 0.3 (pH 7) and 0.1 mM (at lower pH) (Figure 1 C). In all treatments, N_2O was produced but accounted for a maximum of only 0.7% of the NO_2^- consumed. The final N_2O yield per mole NO_2^- reduced tended to be lower in the mineral plus DB versus the mineral-only amended setups for most of the pH (Figure 1 B vs. D). Highest N_2O production was observed at circumneutral pH (7.1) in the mineral-only setup, while maximum final N_2O

concentrations were observed at lower pH (6.2) in the incubations with DB (Figure 1 B; S4). A systematic pH effect, however, could not be discerned. $Fe(II)_{total}$ concentrations rapidly decreased in both setups. In the presence of DB, $Fe(II)_{total}$ oxidation was almost complete (Figure 2A), independent of the pH, whereas in the mineral-only experiment, $Fe(II)_{total}$ decreased during the first 5-10 days but then seemed to reach a steady state (Figure 2 B). At pH 6.8 and 5.8, only 40% of the $Fe(II)_{total}$ was oxidized, whereas at the other pH up to 80% of the $Fe(II)_{total}$ initially amended was oxidized. Total Fe decreased over time (Figure S2).

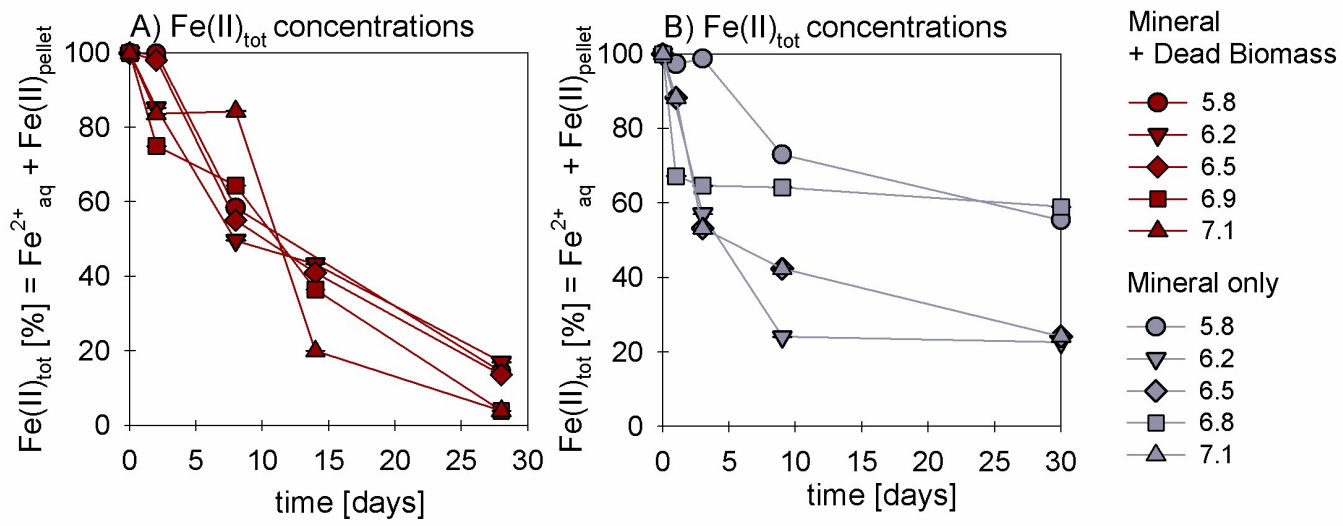

Figure 2: Oxidation of total Fe(II) over time given (reported as % of initial concentration) in the mineral + dead biomass amended (red) and the mineral-only setup (grey), tested at different pH. Standard error calculated from biological replicates (n = 9) is represented by the error bars.

Average rates for NO_2^- reduction and N_2O production at pH 6.8 were calculated (Table 1). Rates were calculated per day and again these results emphasize that the amendment of dead biomass increased the rates by ~92%. Although not complete, Fe(II) oxidation in the presence of DB was also more pronounced leading to only 10.5 ±2.8% Fe(II) remaining compared to the mineral-only setup in which 37.1 ±8.2% Fe(II) remained. To complement the colorimetric data, ^{57}Fe Mössbauer spectroscopy was performed and data are presented in detail in the next section.

Table 1: Chemodenitrification kinetics and mineral transformation during mineral + dead biomass as well as the mineral only experiments. T_{ini} values represent means calculated by summarizing results across all pH ± standard error. Overall reduction/production rates are calculated by subtracting $\overline{[C]}_{t0} - \overline{[C]}_{tend}$ ±standard error/ $\overline{[C]}_{tend} - \overline{[C]}_{t0}$ ±standard error, respectively and are given per day. Fe(III) values are calculated by using ^{57}Fe Mössbauer spectroscopy data. Mineral phases were also identified by using ^{57}Fe Mössbauer spectroscopy with spectra collected at 77 K. Mineral-only sample taken after 28 days was inadvertently destroyed prior to Mössbauer measurement.

	Mineral + Dead Biomass	**Mineral-only**
NO_2^- reduction ($\bar{X}$)	0.053 ±0.013 mmol L^{-1} day^{-1}	0.004 ±0.003 mmol L^{-1} day^{-1}
N_2O production ($\bar{X}$)	353.50 ±32.91 nmol L^{-1} day^{-1}	204.02 ±60.29 nmol L^{-1} day^{-1}
$Fe(II)_{total}$ remaining ($\bar{X}$)	10.54 ±2.77%	37.08 ±8.23%
Fe(III) after NO_2^- addition	7.4%	9.9%
Fe(III) after 28 days	48.7%	*
Mineral phase t_{ini}	Vivianite	Vivianite
Mineral phase t_{end}	Vivianite/Ferrihydrite	*

** Mössbauer sample processing failed*

3.2. Fe mineral analysis

^{57}Fe Mössbauer spectroscopy was used to quantify structural Fe(II) and Fe(III) contents of the samples and identify differences in mineralogy under the different reaction conditions. The hyperfine parameters of the mineral phases in in the mineral-only setup at $t_{initial}$ (pH 6.84) are dominated by Fe(II) doublets (Figure 3 A, QSD Sites 1 and 2), which most closely match that of a vivianite spectrum (Muehe et al., 2013; Veeramani et al., 2011). There is a small component with low centre shift and quadrupole splitting, indicative of Fe(III), which accounts for ~10% of the spectral area (Figure 3 A, QSD Site 3). This suggests some minor oxidation occurred, potentially during transfer of sample into the spectrometer. The mineral phases in the DB-amended setup at $t_{initial}$ (pH 6.89) shows very close approximation to the abiotic mineral-only setup, though with slightly less Fe(III) (~7.5% of the spectral area) (Figure 3 B, QSD Site 2). Precipitates analysed at the end of the DB-amended experiment (Day 28) show that at pH 6.89, the vivianite phase still dominates (Figure 3 C, QSD Sites 1 and 2), however, the Fe(III) component is now much more prominent (Figure 3 C, QSD Site 3), and suggests the formation of a poorly crystalline/short-ranged ordered mineral such as ferrihydrite (Cornell and Schwertmann, 2003). At the lowest pH (5.78) and in the presence of DB, the pattern of the precipitates is completely dominated by one doublet (Figure 3 C, QSD Site 1), with hyperfine parameters corresponding to a poorly ordered Fe(III) mineral such as ferrihydrite (Cornell and Schwertmann, 2003). Unfortunately, the sample processing failed for the mineral-only sample taken after 28 days and can therefore not be used for further elucidations. Detailed fitting results of the ^{57}Fe Mössbauer spectroscopy are provided in Table 2.

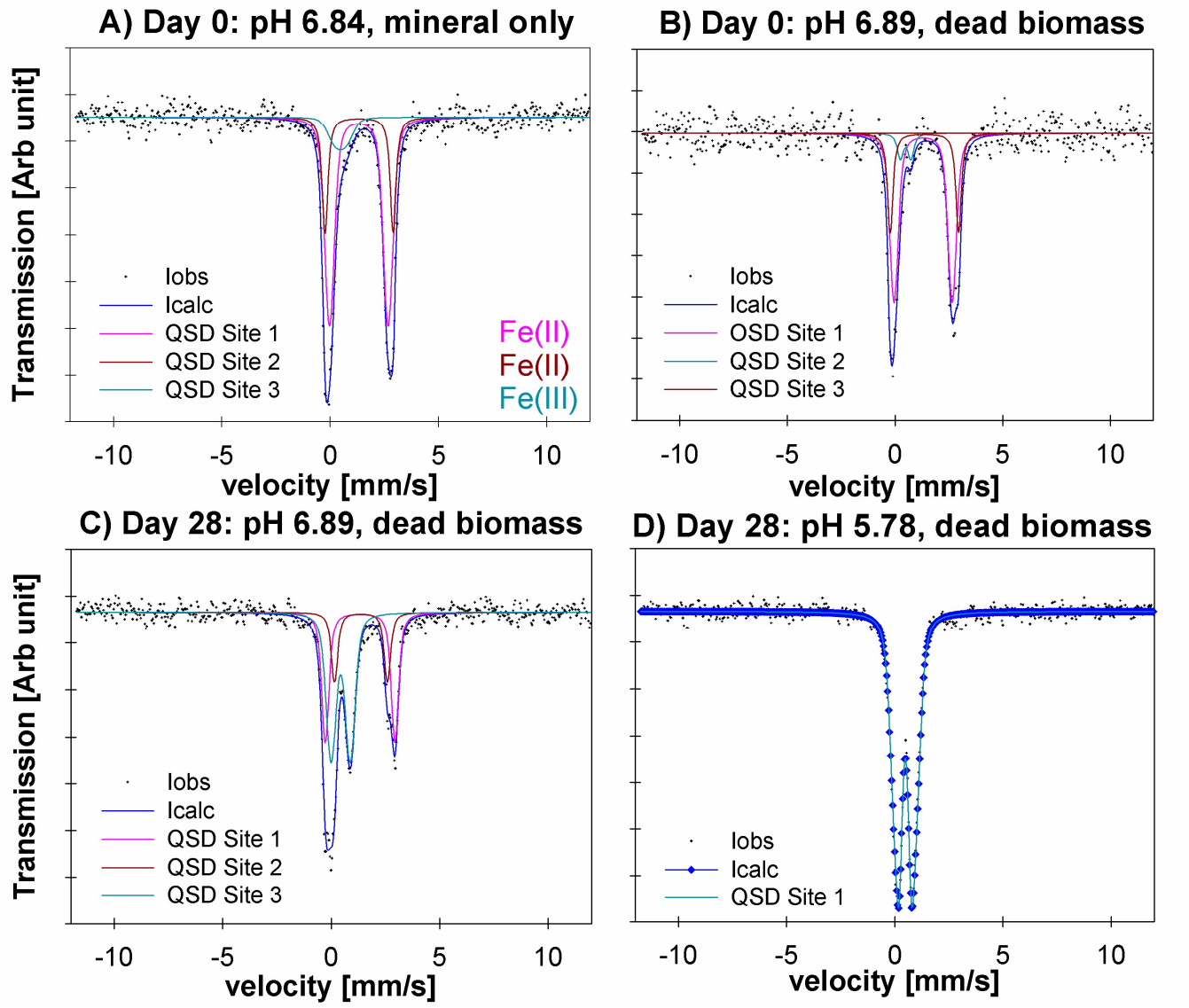

Figure 3: ^{57}Fe Mössbauer spectra collected at 77 K for (A) the mineral only setup precipitates at day 0 and pH 6.84, (B) the mineral + dead biomass amended setup precipitates at day 0 at pH 6.89, (C) the mineral + dead biomass amended setup precipitates at day 28 and (D) the mineral + dead biomass amended setup precipitates at day 28 at pH 5.78. Full lines represent the calculated spectra and their sums. Colours of the fits represent the corresponding Fe phase and thus vary between the graphs: Fe(II) doublets (A, C – QSD Sites 1 and 2, B – QSD Sites 1 and 3) closely match the spectra known for vivianite. Minor amounts of Fe(III) are present at day 0 in both, the mineral-only and DB-amended setups (A/B QSD Site 3/2). Single doublets shown in C (QSD Site 3) and D (QSD Site 1) correspond to a poorly ordered Fe(III) mineral such as ferrihydrite.

Table 2: Fitting results of Mössbauer spectroscopy. CS – centre shift, QS – quadrupole splitting, R.A. – Relative abundance determined by integration under the curve, Chi^2 – goodness of fit; sample collection took place at t_{ini} – initial time point and t_{end} – end time point; MO = mineral-only, MDB = mineral + dead biomass.

Sample	Temp [K]	Phase	CS [mm/s]	QS [mm/s]	R.A. [%]	Error	Chi^2
MO_pH6.8_t_{ini}	77	Fe(II)	1.32	2.71	66.0	23.0	0.55
		Fe(II)	1.33	3.15	24.0	23.0	
		Fe(III)	0.47	0.63	9.9	4.8	
MDB_pH6.8_t_{ini}	77	Fe(II)	1.30	2.70	65.0	14.0	0.68
		Fe(III)	0.49	0.49	7.4	3.6	
		Fe(II)	1.36	3.18	28.0	15.0	
MDB_pH6.8_t_{end}	77	Fe(II)	1.33	3.21	34.3	2.4	0.73
		Fe(II)	1.37	2.44	17.0	2.8	
		Fe(III)	0.44	0.89	48.7	2.4	
MDB_pH5.8 _t_{end}	77	Fe(III)	0.49	0.79	100.0		0.66

3.3. Nitrite and N_2O isotope dynamics

In experiments with DB, the $\delta^{15}N\text{-}NO_2^-$ and $\delta^{18}O\text{-}NO_2^-$ values showed a very consistent initial ~3-4‰-decrease (from -26‰ to -30‰ for $\delta^{15}N$ and from ~+3‰ to 0‰ for $\delta^{18}O$) (Figure 4 A, B). After 5 days, the $\delta^{15}N$ values started to increase again with decreasing NO_2^- concentrations, reaching final values of ~ -20‰ (Figure 4 A), whereas the concomitant increase in the $\delta^{18}O\text{-}NO_2^-$ was much smaller (<1‰, Figure 4 B). The same pattern was observed for all pH levels. In mineral-only experiments, isotope trends were quite different. In combination with far less consumption of NO_2^-, the $\delta^{15}N\text{-}NO_2^-$ values decreased throughout the entire abiotic experiment (Figure 4 C). In contrast, the $\delta^{18}O\text{-}NO_2^-$ first dropped by 2‰, reaching a clear minimum of ~0.5 to -0.5 ‰, before rapidly increasing again. Over the remaining 25 days, the $\delta^{18}O\text{-}NO_2^-$slowly decreased reaching final values of ~1‰ (Figure 4 D) – similar to that of the mineral plus DB treatment.

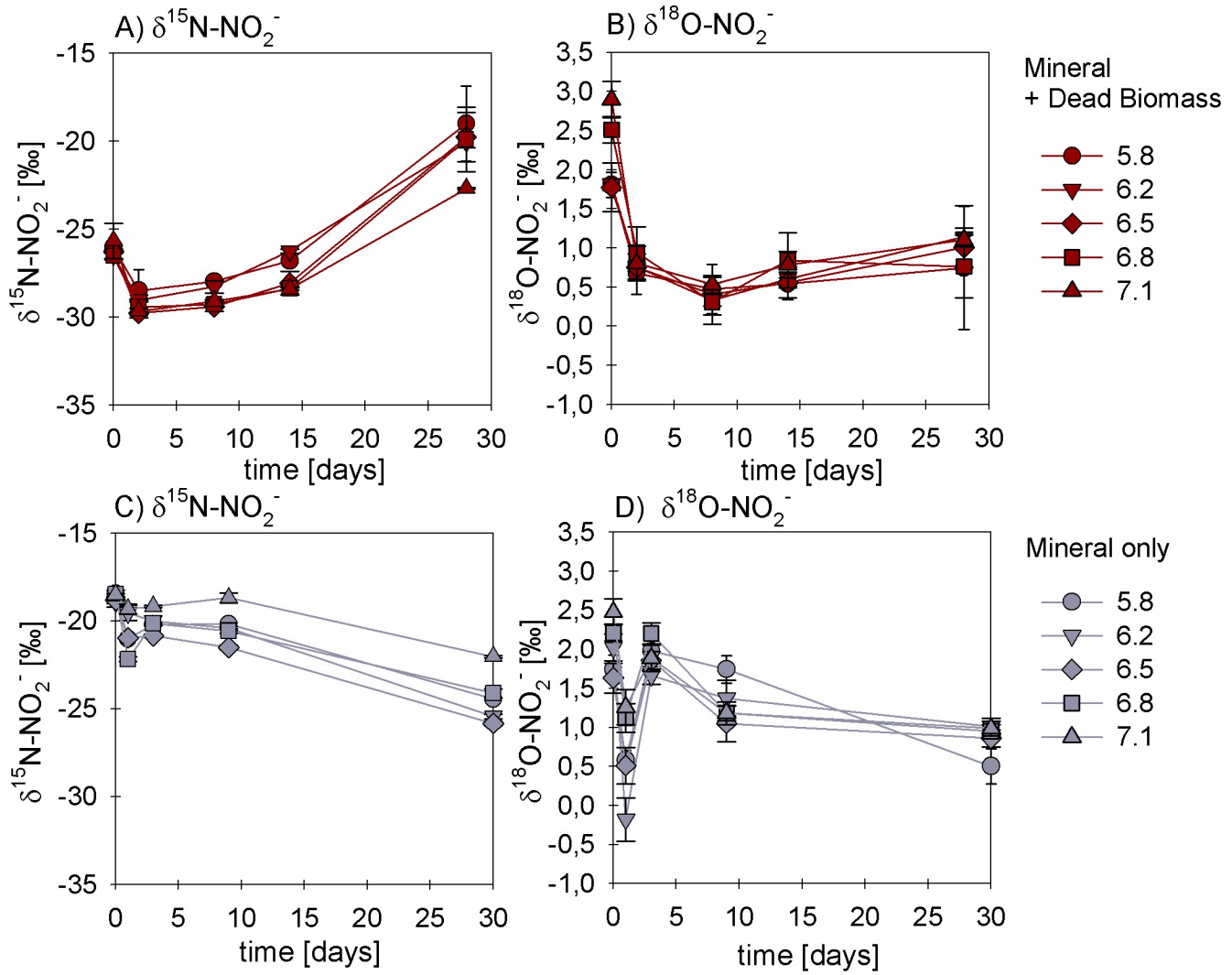

Figure 4: $\delta^{15}N$ (A, C) and $\delta^{18}O$ (B, D) values for NO_2^- measured in the mineral + dead biomass amended (red) and the mineral-only (grey) setups over time and at different pH. Standard error calculated from biological replicates (n = 3) is represented by the error bars.

In order to estimate the net N and O isotope fractionation for putative NO_2^- reduction (in the DB-amended experiments, where we observed a clear decrease in NO_2^-), we plotted the NO_2^- $\delta^{15}N$ and $\delta^{18}O$ values against the natural logarithm of the concentration of the residual NO_2^- (Rayleigh plot), where the slope of the regression line approximates the N and O isotope effects, respectively (Mariotti et al., 1981). At least after the initial period, when the NO_2^- $\delta^{15}N$ markedly increased with decreasing NO_2^- concentrations, the N isotope data are more or less consistent with Rayleigh isotope fractionation kinetics. The slope of the regression line suggests an average N isotope effect of -10.4‰ (Figure 5 A). For the mineral-only setup, no N isotope effect could be calculated, but the observed NO_2^- $\delta^{15}N$ trend suggest a small inverse N isotope fractionation (Figure

4 C). Similarly, trends in NO_2^- $\delta^{18}O$ of the DB experiments are not as obviously governed by normal Rayleigh fractionation dynamics, at least not during the initial period, when the $\delta^{18}O$ decreased despite decreasing NO_2^- concentrations. Considering the $\delta^{18}O$ values only after 2 days of the incubation, the Rayleigh plot revealed an average O isotope enrichment factor of -0.5 ‰ (Figure 5 B), much lower than for N. Similar to N, O-isotope Rayleigh plots for the mineral-only experiments (Figure S5) did not exhibit coherent trends, as the fractional NO_2^- depletion was minor and not consistent (mostly less than 10%). Again, the observed $\delta^{18}O$ minimum at day 2 of the abiotic incubations suggests that processes other than normal kinetic fractionation during NO_2^- reduction were at work, which cannot be described with the Rayleigh model. If at all, the decreasing $\delta^{18}O$ values after day 5 in the mineral-only experiments, accompanying the subtle decrease in NO_2^- concentration in at least some of the treatments, suggest a small apparent inverse O isotope effect associated with the net consumption of NO_2^-. Despite the different NO_2^- $\delta^{18}O$ dynamics during the course of the experiment, the final $\delta^{18}O$ of the residual nitrite was very similar in both experimental setups, and independent of the pH.

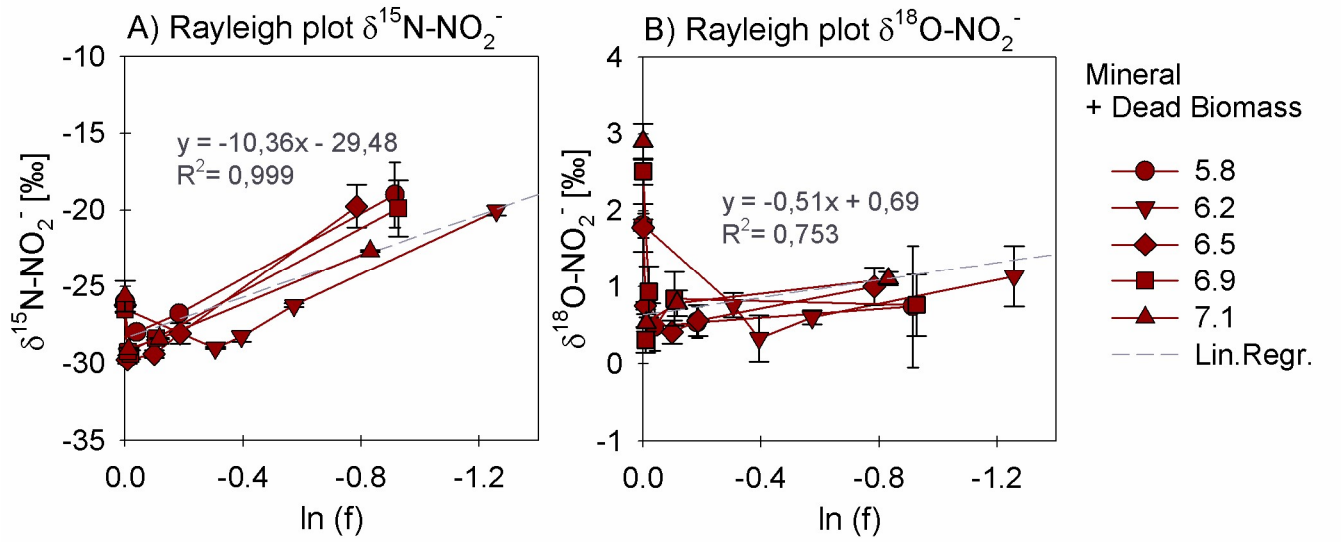

Figure 5: Rayleigh plots for NO_2^- $\delta^{15}N$ (A) and $\delta^{18}O$ (B) values measured for the mineral + dead biomass amended setups over the ln of the substrate fraction remaining and at different pH. The average linear regression line was calculated starting with the lowest delta values (after the initial decrease in both $\delta^{15}N$ and $\delta^{18}O$ during the initial experimental phase). Equation and R^2 are given in grey. Standard error calculated from biological replicates (n = 3) is represented by the error bars.

We also investigated the N_2O isotope dynamics during mineral-only and mineral plus DB incubations. Site preference (SP) and $\delta^{15}N^{bulk}$ of the N_2O produced in both experimental setups were plotted over time (Figure 6 A and B) and show, except for a few values that require further investigation, almost no variation during the period of the experiment. Also, disregarding the rather high and unusual (but well replicated) values already mentioned, the majority of values obtained in both setups indicate that neither pH nor the amendment of DB seems to have had any influence on the isotopic composition of the produced N_2O

(Figure 6 B vs. D). Over the course of the experiment, $\delta^{15}N^{bulk}$ N_2O values were around -50 ±6‰. SP was relatively low, ranging roughly between -4 and a maximum of +14‰ (Figure 6 A, C), without any significant temporal change.

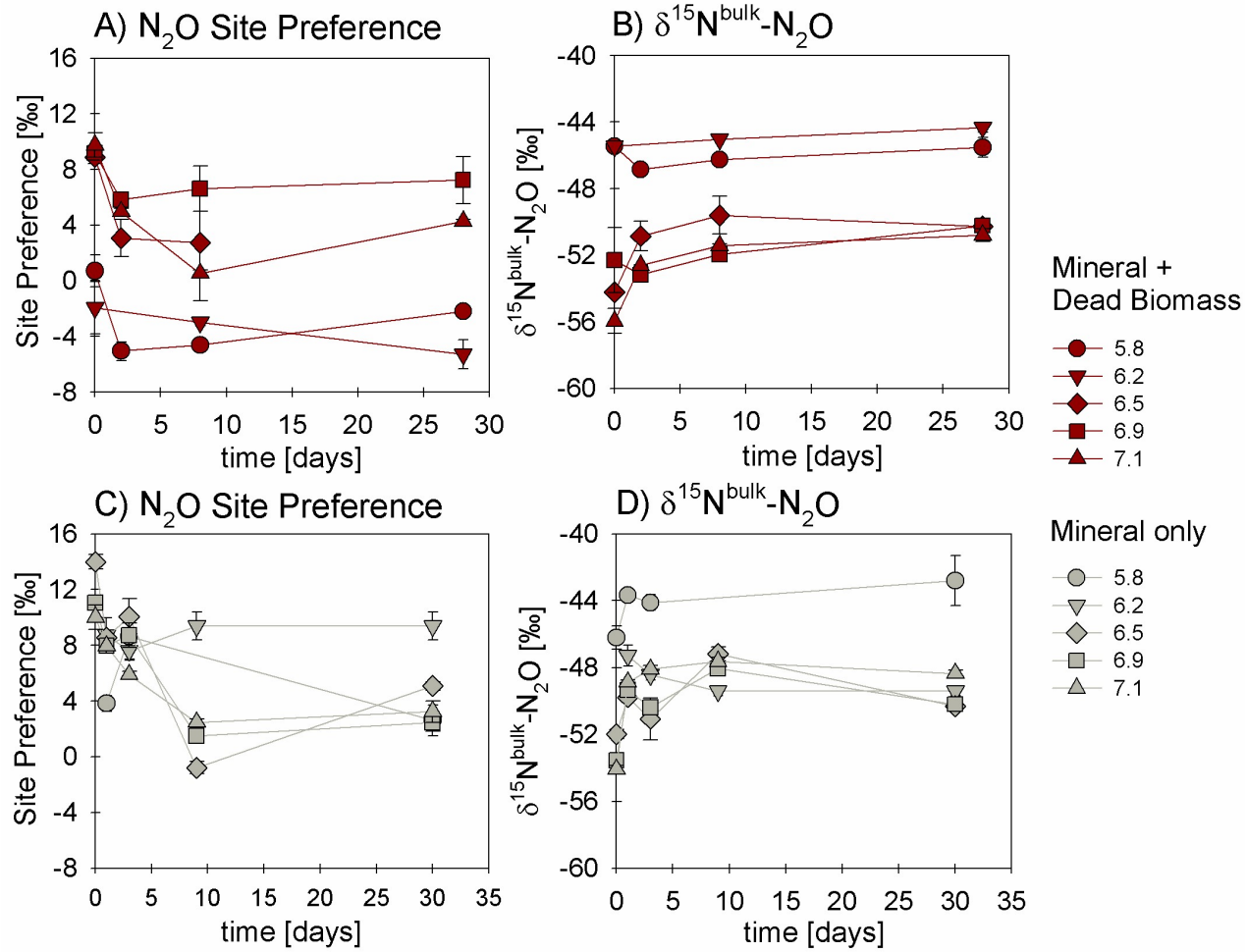

Figure 6: Site Preference (SP; A, C) and $\delta^{15}N^{bulk}$ (B, D) values of N_2O produced in experiments amended with mineral + dead biomass (red) and mineral-only (grey). For pH 6.5, the final SP value (A) is missing due to analytical problems (overly large sample peak areas). Standard error calculated from biological replicates (n = 3 or 2) is represented by the error bars.

Rayleigh diagrams, in which $\delta^{15}N^{\alpha}$, $\delta^{15}N^{bulk}$ and SP of the N_2O were plotted against concentrations of the reactant (NO_2^-) remaining (Figure S6), confirm the similar N_2O isotope dynamics in the DB vs. mineral-only setups, despite the differential degree of NO_2^- reduction (only minor in the mineral-only experiment, with f always greater 0.9) and despite the different NO_2^- N and O isotope dynamics. Similarly, the dual N_2O $\delta^{18}O$ vs. $\delta^{15}N^{bulk}$ signatures (with the exception of two data points; Figure S7) were almost equivalent in both setups, implying that, although modes of NO_2^- reduction clearly differ, a similar mechanism of nitrite-reduction-associated N_2O production exists in both setups. The N and O isotopic results are summarized in Table 3 (see discussion).

4. Discussion and implications

4.1. General evaluation of the abiotic reaction systematics

Overall, the abiotic reaction between NO_2^- and Fe(II), heterogeneous or homogenous, has been considered thermodynamically favourable, and as major contributor to the global N_2O budget (e.g. Jones et al., 2015; Otte et al., 2019). Previous studies on abiotic NO_2^- reduction with Fe(II) have usually been performed in the presence of rather high concentrations (>2 mM) of NO_2^- and/or Fe(II), without taking into account that chemodenitrification is in fact considered to be highly concentration-dependent (Van Cleemput and Samater, 1995). In addition, reaction dynamics were often tested under variable conditions including the presence of different Fe(II)/Fe(III) minerals, sediments, organic materials and/or bacterial cells (Chen et al., 2018; Grabb et al., 2017; Otte et al., 2019). Whether NO_2^- indeed acts as a direct oxidant of Fe(II) at circumneutral pH or whether the reaction requires catalysis is still a matter of debate (Kampschreur et al., 2011; Sorensen and Thorling, 1991).

Integrating concentrations that are pertinent to our experiments, we constructed a Pourbaix diagram (e.g. Delahay et al., 1950; Minguzzi et al., 2012) (Figure 7). Based on these (simplified) thermodynamic calculations, the abiotic reaction solely driven by the reaction of NO_2^- and aqueous Fe^{2+} at a pH range of 5 to 7 is not supported. Under our experimental conditions, Fe^{2+} is predicted to be oxidized by NO rather than NO_2^-. Considering Figure 7, an accumulation of NO at µM or even mM concentrations would result in a downward shift of the NO_2^- line. Therefore, an accumulation of NO would only lower the reactivity between NO_2^- and Fe^{2+}, which implies that NO_2^- is not oxidizing Fe^{2+}. Again, this also implies that the reactivity between NO_2^- and Fe^{2+} is only enhanced if NO concentrations are rather low (pM range). In order to avoid NO accumulation and thus to enhance the abiotic reaction between NO_2^- and Fe^{2+}, NO would need to react further (either with Fe^{2+} or otherwise). This would induce a reaction cascade, resulting in the constant reduction of NO_2^- and NO, and thus in higher N_2O concentrations. In contrast, if NO does accumulate as previously reported, the reaction between NO_2^- and Fe^{2+} would be suppressed and only NO could be reduced further to N_2O, a reaction that of course also depends on gas equilibration dynamics occurring with the headspace of the system. Nevertheless, considering all these aspects, including the fact that the N_2O produced corresponds only to a minor fraction of the initial NO_2^- reduced, NO acting as main oxidizing agent seems more likely. The reaction mechanisms in this system are, however, complex and we note that this simplified thermodynamic analysis does neglect catalytic effects that are possibly induced by reactive surfaces. The complexity of this system is further indicated by the fact that, according to the Pourbaix diagram, a pH response towards N_2O accumulation would be expected which has, however, never been reported so far. Furthermore, testing various pH did not reveal an obvious pH effect on the reaction dynamics. Changes in pH will most certainly affect interactions between species such as HNO, NO_2 and N_2O and thus could impact the reaction dynamics. It appears that, for a more detailed understanding of this redox system, the reactants/intermediates involved and thus the specific reaction kinetics would need to be determined. Unfortunately, quantification of these intermediates is hampered by their high reactivity, transient nature, and lack of detection techniques that can be applied in batch culture experiments. Since low amounts (e.g., pM) of NO suffice to impact reaction dynamics and thus stimulate the reaction between NO_2^- and Fe^{2+}, NO quantification could be crucial to assess the environmental controls on

Fe(II)-coupled chemodenitrification. In laboratory biological denitrification experiments, accumulation of NO has been reported (Goretski and Hollocher, 1988; Zumft, 1997) and was shown to even account for up to 40% of the initial NO_3^- amended (Baumgärtner and Conrad, 1992; Choi et al., 2006; Kampschreur et al., 2011; Ye et al., 1994; Zumft, 1997). Hence, Kampschreur et al., (2011) concluded that chemodenitrification is not necessarily solely caused by a single-step reaction, and proposed that the oxidation of Fe^{2+} is rather caused by a two-step mechanism. They observed an immediate formation and accumulation of NO after NO_2^- was added to Fe^{2+}, and as soon as a considerable fraction of the Fe^{2+} was oxidized, N_2O formation was detected. Although NO and other possible intermediate (e.g. $NO_2(g)$) concentrations might not play a major role with regard to mass balance considerations, their possible impact on the overall reaction systematics as well as the isotopic fractionation, remains unclear.

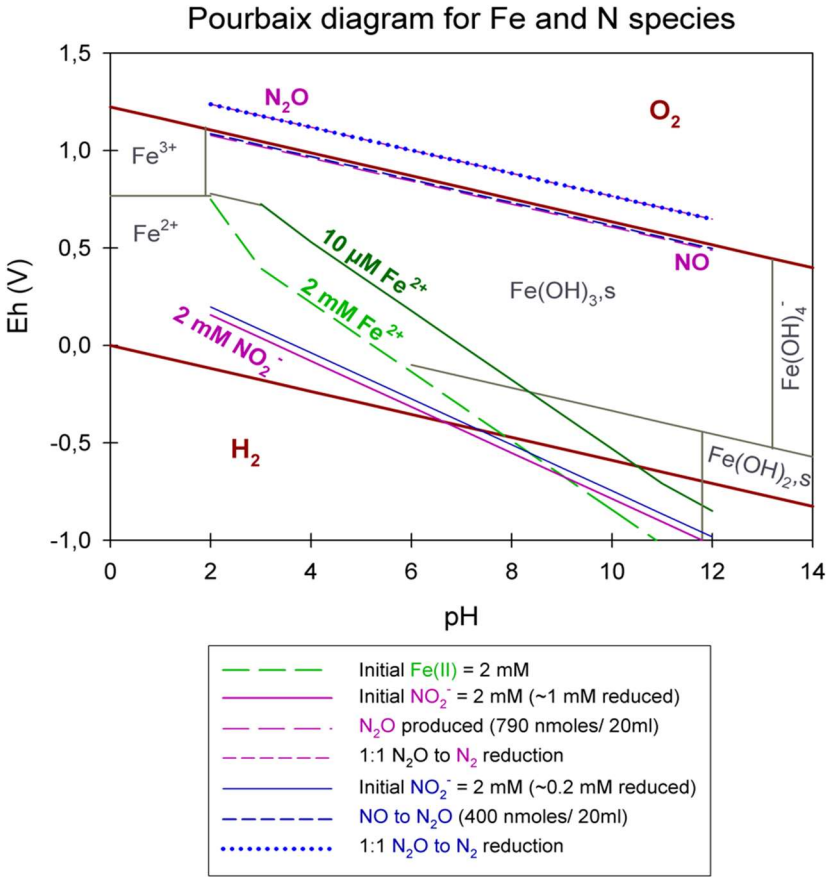

Figure 7: Pourbaix diagram depicting an Fe and N-species based system. Overall calculations are based on the Nernst equation using values taken from literature (for equation and values see table S1). Green lines represent Fe^{2+} concentrations, pink lines represent NO_2^- reduction experiments, starting with 2 mM NO_2^-, resulting in the reduction of 1 mM NO_2^-, the production of 790 nmol /20 ml N_2O and a 1:1 transformation of N_2O to N_2; blue lines represent NO_2^- reduction experiments, starting with 2 mM NO_2^-, resulting in the reduction of 0.2 mM NO_2^-, the production of 790 nmol /20 ml N_2O and a 1:1 transformation of N_2O to N_2. Reduction/production values were taken from our results presented in 3.1.

4.2. Surface catalysis of chemodenitrification

Previous studies have shown that the initial presence of either Fe(III)(oxyhydr)oxides (Coby & Picardal, 2005; Klueglein & Kappler, 2013; Sorensen & Thorling, 1991) or amorphous Fe(II) minerals (Van Cleemput and Samater, 1995) can stimulate the abiotic reaction between NO_2^- and Fe^{2+}. As summarized in Table 1, under mineral-only conditions NO_2^- reduction was significantly lower (0.004 ±0.003 mmol L^{-1} day^{-1}) than in identical experiments containing DB, which substantially enhanced NO_2^- reduction (0.053 ±0.013 mmol L^{-1} day^{-1}). The catalytic effect of Fe minerals on the abiotic NO_2^- reduction, which has been demonstrated before, seems to be amplified in the presence of DB. Relative to NO_2^- reduction rates, overall final N_2O yields per mole NO_2^- reduced tended to be higher in the mineral-only setups. However, considering the initial NO_2^- concentrations, only minor amounts of N_2O were produced in both setups, raising questions about the contribution of chemodenitrification to global N_2O emissions discussed by others (Grabb et al., 2017; Jones et al., 2015; Otte et al., 2019; Zhu-Barker et al., 2015). For example, in comparison to the N_2O yields in experiments where chemodenitrification was catalysed by green rust (up to 31%, Grabb et al., 2017), the amount of N_2O produced in our setups is far lower (<5% of the initial NO_2^-).

Fe-bearing minerals are known for their high reactivity, ability to complex ligands (metals, humics) and phosphates, and surface protonation capacity via the sorption of OH^- groups (Elsner et al., 2004; Stumm and Sulzberger, 1992). Surface catalytic effects may include *direct* and *indirect* sorption-induced catalysis. In the environment, pH has been shown to have a strong influence on these sorption capacities of Fe minerals in general (Fowle and Konhauser, 2011). Considering the point of zero charge (PZC) of vivianite, which is with 3.3 below the lowest tested pH in our experiments, the mineral surface is positively charged under our experimental conditions (Luna-Zaragoza et al., 2009). Hence the pH range tested here will not affect the surface charge, and NO_2^- sorption onto mineral surfaces and corresponding heterogeneous reactions are possible. In contrast, cell surfaces are considered to be negatively charged (Wilson et al., 2001) and therefore might induce different effects than mineral surfaces. The charge of the cell surface most likely remained negative even after autoclaving (see e.g. Halder et al., 2015). Our results imply that the systematics of chemodenitrification are strongly dependent on the surface provided and that, depending on the availability and quality of catalytic surfaces, Fe coupled chemodenitrification may be a single-step reaction (between NO_2^- and Fe) or may occur in multiple steps (reaction between Fe and NO_2, as well as Fe and NO). As a consequence, the nature of surface catalysis would likely have a strong impact on the N_2O yield per mole NO_2^- reduced to NO. Since NO has been demonstrated to have a strong affinity towards Fe^{2+} and Fe^{3+} centres resulting in the formation of $Fe^{x+}(NO)_n$ nitrosyls and thus triggering an enhancement of the N_2O decomposition rate (e.g. Rivallan et al., 2009). It remains unclear to what extent, and why, the quality of the catalytic surfaces plays a role. Particularly in the presence of organics and/or dead bacterial cells, which are known to have a high affinity to bind metal ions (e.g. Ni^{2+}, Cu^{2+} or Zn^{2+}), either directly or by forming surface complexes with hydroxyl groups (Fowle and Konhauser, 2011), a surface-catalysis-induced reaction can be expected. Besides acting as a catalyst via a reactive surface, the dead biomass might also have directly triggered the reaction. For example, non-enzymatic NO formation was studied and modelled by Zweier et al. (1999), suggesting that at concentrations

between 100 and 1000 µM, abiotic NO_2^- disproportionation and thus NO formation at circumneutral pH in organic tissue is still possible (Zweier et al., 1999). Furthermore, autoclaving might have ruptured cell walls and released organic compounds. In the presence of phenolic compounds, humic substances, and other organic compounds, NO_2^- has been shown to form NO via self-decomposition (Nelson and Bremner, 1969; Stevenson et al., 1970; Tiso and Schechter, 2015). Whether this may have been the case also in our experiments remains unclear, since we did not conduct experiments containing only DB and NO_2^-. Another possible consideration is the presence of extracellular polymeric substances (EPS), which should also be tested in future studies. Liu et al., (2018) investigated nitrate-dependent Fe(II) oxidation with *Acidovorax* sp. strain BoFeN1, showing that *c*-cytochromes were present in EPS secreted which could indeed act as electron shuttling agents involved in electron transfer supporting chemolithotrophic growth. Since *S. oneidensis*, our model organisms used as DB supply, is known to produce large amounts of EPS, harbouring *c*-cytochromes (Dai et al., 2016; Liu et al., 2012; White et al., 2016), a potential impact of EPS on the reaction between NO_2^- and Fe(II) needs to be considered. However, possible cytochromes present in the EPS most likely lost their activity due to protein denaturation during autoclaving (Liu & Konermann, 2009; Tanford, 1970). Nevertheless, EPS is still present and can act as a catalysing agent to the abiotic reaction mechanism (Klueglein et al., 2014; Nordhoff et al., 2017).

$Fe(II)_{total}$ oxidation via NO_2^- has also been observed in the mineral-only setups, but to a lower extent. Hence, the vivianite mineral surfaces themselves seem to catalyse the abiotic reaction between NO_2^- and Fe(II)/ Fe^{2+} (in parts, the stimulation of Fe-dependent nitrite reduction may also be attributed vivianite dissolution providing ample Fe(II) substrate). Previous studies reported on mineral-enhanced chemodenitrification (Dhakal et al., 2013; Grabb et al., 2017; Klueglein & Kappler, 2013; Rakshit et al., 2008), and the catalytic effect may be due to NO_2^- adsorption onto the minerals surface possibly facilitating a direct electron transfer. Similar findings have been reported previously on Fe(II) oxidation promoted by electron transfer during adsorption onto a Fe(III) minerals surface (Gorski and Scherer, 2011; Piasecki et al., 2019). OH^- adsorption is probably enabled by the minerals positive surface charge at pH >6, resulting in a limited reactive surface availability. Complexation of dissolved Fe^{2+}, which is provided by mineral dissolution, by OH^- groups would thus result in a lower overall NO_2^- reduction rate compared to the DB-amended setups. Nevertheless, the NO formed by the initial NO_2^- reduction could, at still elevated Fe^{2+} levels, proceed until both dissolved and adsorbed Fe(II) is quantitatively oxidized to surface-bound Fe(III) (Kampschreur et al., 2011). This would ultimately lead to similar $Fe(II)_{total}$ oxidation and N_2O production (and thus higher N_2O yields) as in the DB amended experiment and thus explain the similar results.

4.3. Mineral alteration during Fe-coupled chemodenitrification

We used ^{57}Fe Mössbauer spectroscopy in order to determine, whether the catalytic effects that enhanced chemodenitrification with Fe^{2+} also modulated mineral formation. In both setups, addition of $Fe(II)Cl_2$ to the 22 mM bicarbonate buffered medium led to the formation of vivianite, an Fe(II)-phosphate. Shortly after the addition of Fe^{2+}_{aq}, the mineral phase in both setups was dominated by Fe(II), but a small fraction of Fe(III) was also present. Initial fractions of Fe(III) were similar in both the mineral-only and DB-amended experiments (9.9% and 7.4%, respectively) and, if not an artefact of Mössbauer sample handling, might

therefore have stimulated Fe(II) adsorption and oxidation (Gorski and Scherer, 2011; Piasecki et al., 2019). The reduction of NO_2^- was accompanied by a marked increase of Fe(III), likely in the form of short-range ordered ferrihydrite or lepidocrocite. Thus, the Fe(III) phase detected at day 0 most likely formed immediately after NO_2^- addition. This is supported by prior studies, which demonstrated the initiation of Fe(II) oxidation with NO_2^- within a short period of time (Jamieson et al., 2018; Jones et al., 2015). At the end of the DB experiment at pH 6.89, oxidized Fe(III) (most likely in the form of poorly ordered ferrihydrite) contributed 48.7% to the total Fe phases, with vivianite accounting for the remaining spectral area. Unfortunately, we are unable to compare the results of the DB-amended precipitates at the end of the experiment to the mineral-only setup, since the sample processing failed. Minerals obtained from the enrichment culture KS were mostly vivianite and ferrihydrite, which is, however, attributed to the fact that for the cultivation of the KS culture a high-phosphate medium is used (Nordhoff et al., 2017). In the abiotic experiments (10 mM Fe(II) and 10 mM NO_2^-) presented by Jones et al., (2015), the formation of lepidocrocite, goethite and two-line ferrihydrite were observed after 6 to 48 hrs. In the experiments presented here, besides a short-range ordered Fe(III) phase, likely ferrihydrite, no other mineral phases could be identified after 28 days.

Iron analysis also indicates that the oxidation of the $Fe(II)_{total}$ went to completion at pH 5.8 whereas at pH 6.8, 52.3% of the $Fe(II)_{total}$ remained at the end of the incubation experiment, resulting in the formation of a poorly-ordered ferrihydrite. Unfortunately, we did not measure the zeta potential of the starting solutions, which would probably help to explain the differences detected. We note that, although ^{57}Fe Mössbauer spectroscopy was used to measure the Fe(II)/Fe(III) in the precipitates, the reported $Fe(II)_{total}$ concentrations reflect the total Fe(II), i.e., of both the dissolved pellet (structurally-bound or adsorbed) and the aqueous Fe^{2+} in the supernatant measured by ferrozine. The results obtained by Mössbauer analysis (50% Fe(II) remaining) seem to contradict the ferrozine assay (<10% remaining) (see Table 1 and 2). The presence of ferrous Fe, either as structurally-bound Fe(II) or adsorbed Fe^{2+} does indeed play a crucial role with regards to the reaction dynamics occurring at the mineral surfaces, particularly if we assume that N-reactive species are also still present (Rivallan et al., 2009). In addition, the initially formed Fe(III) phase might also induce another feedback to the N and even the Fe cycle since Fe(III) minerals are also highly reactive (Grabb et al., 2017; Jones et al., 2015). Mineral structure and thus Fe(II) location within the lattice can influence the overall Fe accessibility, the binding site at the mineral surface and thus overall reactivity (Cornell and Schwertmann, 2003; Luan et al., 2015; Schaefer, 2010). If the initial formation of Fe(III), however, enhanced the reaction between NO_2^- and Fe(II), similar results in both setups should have been observed, which this was not the case since NO_2^- reduction patterns in the mineral-only experiments were much lower. This also indicates again, that the presence of DB indeed contributed greatly to the reaction in the DB experiments. Furthermore, results obtained from Mössbauer analysis are the only results supporting a pH-dependent effect: At pH 5.78 and in the presence of DB, all vivianite was fully transformed into a short-range ordered Fe(III) phase whereas at pH 6.89, vivianite remained a major component. This presence of vivianite also indicates that no further Fe(II) oxidation occurred even though NO_2^- reduction was incomplete. The incomplete reduction of NO_2^- in turn suggests that further Fe(II) oxidation was limited due to blocked or deactivated reaction sites on mineral surfaces. Also, considering that at pH 5.8 and in the presence of DB, the initial NO_2^- concentrations were higher but the overall reaction

493 dynamics were quite similar to the other reaction conditions, the concentration dependency of the reaction between NO_2^- and
494 Fe(II) is again supported.

495 **4.4. Nitrite and N_2O N and O isotope dynamics during chemodenitrification**

496 In the presence of only vivianite, a decrease in $\delta^{15}N\text{-}NO_2^-$ of ~3‰ occurred in parallel with initially decreasing NO_2^-
497 concentrations. Initial $\delta^{18}O\text{-}NO_2^-$ values also reflect this drop of 3‰ during the first 3 days but level off and stabilize at 1‰
498 after 9 days. The initial decrease in both $\delta^{15}N$ and $\delta^{18}O$ of NO_2^- suggest apparent inverse isotope effects, which to the best of
499 our knowledge have never been observed during chemodenitrification, and have only been reported for enzymatic NO_2^-
500 oxidation (Casciotti, 2009). Since biological NO_2^- oxidation can be ruled out (no NO_3^- produced, no microbes), the decrease
501 in $\delta^{15}N\text{-}NO_2^-$, though subtle, could indicate that either heavy isotopes are incorporated in the products formed (i.e. NO, N_2O),
502 at least at the beginning of the incubation period. Normally, the heavier isotopes build compounds with molecules of higher
503 stability (Elsner, 2010; Fry, 2006; Ostrom & Ostrom, 2011). This is particularly true for the formation of some minerals or
504 highly stable molecules that are formed under mineral-only conditions, where processes can reach an isotopic equilibrium (He
505 et al., 2016; Hunkeler & Elsner, 2009; Li et al., 2011; Ostrom & Ostrom, 2011). However, in the system presented here, N
506 incorporation into mineral phases can be excluded, hence another process must favour the heavy N-atoms. Since this initial
507 drop in $\delta^{15}N$ was also observed in the DB-amended experiments, a possible explanation might be that the isotope values here
508 reflect the sorption or complexation mechanism of NO_2^- onto the reactive surfaces. In contrast $\delta^{18}O\text{-}NO_2^-$ values, after the
509 initial decrease, did not change greatly with decreasing NO_2^- concentrations. The stabilization of the $\delta^{18}O\text{-}NO_2^-$ towards the
510 end of the experiment most likely reflects the oxygen isotope equilibration between $\delta^{18}O\text{-}NO_2^-$ and the $\delta^{18}O$ of the water in the
511 medium. Temporal $\delta^{18}O\text{-}NO_2^-$ dynamics did not change greatly between the different pH treatments, and in all cases the final
512 $\delta^{18}O\text{-}NO_2^-$ ranged between 0.5 and 1‰. The kinetics of abiotic O-atom exchange is a function of temperature and pH. At near
513 neutral pH, at room temperature, one can expect NO_2^- to be fully equilibrated after two to three days (Casciotti et al., 2007).
514 At higher pH, the first order rate constants for the equilibration with water are lower (Buchwald and Casciotti, 2013), but
515 equilibrium conditions should have been reached well within the incubation period. Indeed, the final $\delta^{18}O\text{-}NO_2^-$ was consistent
516 with an equilibrium O isotope effect between NO_2^- and H_2O with a $\delta^{18}O$ of ~ -11.5‰ (Buchwald and Casciotti, 2013). With
517 regards to $\delta^{15}N\text{-}NO_2^-$ values of the DB-amended experiments, a similar behaviour is found within the first 3 days (i.e., decrease
518 in $\delta^{15}N$), followed by a clear increase in $\delta^{15}N\text{-}NO_2^-$ of ~10‰. While it is difficult to explain the initial decrease in $\delta^{15}N\text{-}NO_2^-$
519 (a feature that was not observed in other chemodenitrification experiments (i.e. Grabb et al., 2017; Jones et al., 2015), the
520 subsequent increase in $\delta^{15}N$ can be attributed to normal isotopic fractionation associated with chemodenitrification and an N
521 isotope effect (-9‰) that is consistent with those previously reported on Rayleigh-type N and O isotope kinetics during
522 chemodenitrification with Fe(III)-bearing minerals such as nontronite and green rust (Grabb et al., 2017). In contrast, $\delta^{18}O\text{-}$
523 NO_2^- values initially decrease as in the abiotic experiment but then level off faster reaching final values of ~1‰, again most
524 likely explained by O atom isotope exchange pulling the $\delta^{18}O\text{-}NO_2^-$ values towards the O-isotope equilibrium value. This value
525 is given by the $\delta^{18}O_{H2O} + {}^{18}\varepsilon_{eq,NO2-}$, whereas the latter is defined as the equilibrium isotope effect between NO_2^- and H_2O and

has been shown to yield values of roughly +13‰ (Casciotti et al., 2007). Overall, it seems that the non-linear behaviour of the NO_2^- in the O isotope Rayleigh plot is most likely due to the combined effects of kinetic O isotope fractionation during NO_2^- reduction, and O atom exchange between NO_2^- and H_2O.

NO_2^- N and O isotope trends observed under the DB-amended conditions (in which a large portion of the NO_2^- pool was consumed), somewhat contradict prior reports of chemodenitrification exhibiting a clear increase in both $\delta^{15}N$ and $\delta^{18}O\text{-}NO_2^-$, with N isotope enrichment factors for NO_2^- reduction between -12.9 and -18.1‰ and an O isotope effect of -9.8‰ (Jones et al., 2015). Consistent with our data, however, they also observed that, at least in abiotic experiments where NO_2^- consumption is rather sluggish due to Fe^{2+} limitation (as a result of either oxidation or simply occlusion), O-isotope exchange isotope effects mask the effects of kinetic O isotope fractionation. While we cannot say at this point what exactly governs the combined NO_2^- N vs. O isotope trends in the two different experimental conditions, we observed that the two processes (water isotope equilibrium and KIE) competing with each other lead to different net dual isotope effects. Our data cannot resolve whether these observations reflect fundamental differences or simply changes in the relative proportion of the competing processes. Nevertheless, our observations may still be diagnostic for chemodenitrification catalysed by a mineral surface on the one hand, and Fe-coupled chemodenitrification that involves catalytic effects by dead bacterial cells on the other. The mineral catalyst evidently plays an important role with regards to chemodenitrification kinetics, reaction conditions, surface complexation or contact time between the NO_2^- substrate and the mineral phase (Samarkin et al., 2010), and in turn the combined kinetic/equilibrium N and O isotope effects.

The $\Delta^{15}N$ values ($\Delta^{15}N = \delta^{15}N_{nitrite} - \delta^{15}N_2O^{bulk}$) presented in Table 3 were obtained by subtracting the average $\delta^{15}N^{bulk}$ value of N_2O (abiotic -49.5 ±0.6‰; dead biomass -50.5 ±0.8‰) across all pH and throughout the experiment from the average of the initial $\delta^{15}N_{nitrite}$ value. These values can provide insight on reaction kinetics between NO_2^-, NO, and N_2O (Jones et al., 2015). In both setups there is an offset between the NO_2^- and N_2O $\delta^{15}N$, which is clearly higher than what would be expected based on the NO_2^- reduction NO_2^- isotope effect of <10‰. Following the argumentation of Jones et al. (2015), who reported a similar N isotopic offset between NO_2^- and N_2O of 27.0 ±4.5‰, this could be indicative for a heavy N accumulating in a forming NO pool, whereas ^{14}N is preferentially reacting to N_2O or N_2, respectively. This might even be supported by the rather low $\delta^{15}N^{bulk}$ values detected for N_2O in both setups.

Table 3: Comparison of the isotope values obtained during dead biomass versus the abiotic experiments. t0 values represent means calculated by summarizing results across all pH ± standard error. $\delta^{15}N$ and $\delta^{18}O$ values were calculated using $\bar{x}_{t0} - \bar{x}_{tend}$, whereas an overall increase from the initial value is marked with ↑, and a decrease with ↓. The calculated isotope fractionation factor (ε) is based on the slope between the lowest initial value (here at t_1) and t_{end} for all pH. $\Delta^{15}N$ (= $\delta^{15}N_{nitrite}$ - $\delta^{15}N_2O^{bulk}$) was calculated for the end of the experiment.

	Dead Biomass	Abiotic
$\delta^{15}N_{nitrite}(t_0\text{-}t_{end})$	↑5.99 ±0.65‰	↓5.93 ±0.73‰
$\delta^{18}O_{nitrite}(t_0\text{-}t_{end})$	↓1.75 ±0.23‰	↓1.15 ±0.18‰
$^{15}\varepsilon_{nitrite}$	-10.36 ‰[#]	-
$^{18}\varepsilon_{nitrite}$	-0.51‰[#]	-
SP	2.3 ±1.2‰	6.5 ±0.8‰
$\delta^{15}N^{\alpha}$	-48.9 ±0.1‰	-46.3 ±0.06‰
$\delta^{15}N^{bulk}$	-50.5 ± 0.8‰	-49.5 ±0.6‰
$\Delta^{15}N$	24.4‰	30.9‰

[#] n=4 (t1 to tend); - concentrations in abiotic experiment fluctuate and show only minor decrease, hence $^{15}\varepsilon$ and $^{18}\varepsilon$ could not be calculated.

While our results clearly showed that N_2O accumulates over the course of the reaction, it remains unclear, which additional end products are present at the final stage of the experiment. If NO accumulates (instead of following the reaction cascade further), the substrate-product relationship between the $\delta^{15}N\text{-}NO_2^-$ and $\delta^{15}N\text{-}N_2O$ values that would be expected in a closed system is perturbed, leading to significantly higher $\Delta^{15}N$ than predicted by the $\delta^{15}N\text{-}NO_2^-$ trend. Hence, the calculated $\Delta^{15}N$ of the mineral-only treatment (30.9‰) is slightly higher than that of the DB experiment (24.4‰), and would therefore suggest that despite the differences in chemodenitrification kinetics (i.e. different NO_2^- reduction rates and extent), the NO pool formed is enriched in heavy N in both treatments, respectively. Alternatively, fractional reduction of the produced N_2O to N_2 may also affect the $\Delta^{15}N$ since it would presumably increase the $\delta^{15}N\text{-}N_2O$ and thereby raise the low $\delta^{15}N\text{-}N_2O$ closer to the starting $\delta^{15}N\text{-}NO_2^-$. Abiotic decomposition of N_2O to N_2 in the presence of Fe-bearing zeolites has been investigated previously (Rivallan et al., 2009), however, it remains unclear if this process could also occur here. Fractional N_2O reduction is also not explicitly indicated by the SP values, which would reflect an increase with N_2O reduction (Ostrom et al., 2007; Winther et al., 2018). The SP values in both mineral-only and DB-amended experiments were, with some exceptions, relatively low (6.5 ± 0.8‰; 2.3 ± 1.2‰; Fig. 6, Table 3). In fact, SP values observed during the course of our experiments are significantly lower compared to SP values reported in other studies on Fe-oxide-mineral associated chemodenitrification (e.g. ~16‰; Jones et al. (2015); 26.5‰; Grabb et al. 2017), or during the abiotic N_2O production during the reaction of Fe and a NH_2OH/NO_2^- mixture (34‰; Heil et al. 2014). While the variety of different SP values for chemodenitrification-derived N_2O suggests different reaction conditions and catalytic effects, our SP data seem to imply that the mineral catalyst plays only a minor role with regards to the isotopic composition of the N_2O produced. However, since N_2O concentrations, even if minor, are increasing towards the end of the experiments, production and possible decomposition as well as ongoing sorption mechanisms might

also serve as possible explanation leading to these rather low SP values. N_2O SP values have been used as valuable tracer for microbial N_2O production (Ostrom & Ostrom, 2012). Based on pure culture studies (Ostrom et al., 2007; Winther et al., 2018; Wunderlin et al., 2013) and investigations in natural environments (Wenk et al., 2016) a SP range of -10 to 0‰ is considered to be characteristic for denitrification or nitrifier-denitrification (Sutka et al., 2006; Toyoda et al., 2005), whereas higher values are usually attributed to nitrification or fungal denitrification (Ostrom & Ostrom, 2012; Wankel et al., 2017; Well & Flessa, 2009). The SP values reported here (0 to 14‰) fall well within the range of biological N_2O production, explicitly denitrification and soil derived denitrification (2.3 to 16‰) (Ostrom & Ostrom, 2012), rendering the separation between chemodenitrification and microbial denitrification based on N_2O isotope measurements difficult, if not impossible.

In summary, the N and O isotope systematics of chemodenitrification are multifaceted, depending on the environmental conditions, reaction partners provided, and/or the speciation of precipitated mineral phases. The systematics observed here are clearly not entirely governed by normal kinetic isotope fractionation only, as has also been observed in previous work. Grabb et al. (2017) demonstrated that there is a relationship between reaction rate and kinetic NO_2^- N and O isotope effects, with faster reaction leading to lower $^{15}\varepsilon$ and $^{18}\varepsilon$. Again, changes in the expression and even in the direction of the isotope effects in the NO_2^- pool suggest that multiple processes, including equilibrium isotope exchange (at least with regards to the $\delta^{18}O$- NO_2^-), are contributing to the net N and O isotope fractionation regulated by the experimental conditions and reaction rates. As pointed out by Grabb et al. (2017), and as supported by our comparative study with pure abiotic mineral phases and with added dead biomass, the accessibility of Fe(II) to the reaction may be a key factor regarding the degree of N and O isotope fractionation expressed, particularly if complexation limits the reactive sites of the mineral. The conditions that, at least transiently, lead to the apparent inverse N and O isotope fractionation observed here for chemodenitrification requires particular attention by future work. At this point, we can only speculate about potential mechanisms, which are indicated in the conceptual illustration (Figure 8). As chemodenitrification seems to be catalysed by reactive surfaces of Fe(II)/Fe(III)-minerals and/or organics (including cells), sorption onto these surfaces might play a crucial role in the fractionation of N and O isotopes. For example, during the catalytic hydrogenation of CO_2 on Fe and Co catalysts, a subtle depletion (ca. 4‰) in $^{13}CO_2$ at progressed conversion to methane has been explained by the precipitation of a ^{13}C-enriched carbon intermediate (e.g., CO-graphite) on the catalyst surface (Taran et al., 2010). We are fully aware that it is difficult to compare our system with Fischer-Tropsch synthesis of methane occurring at high temperature and pressure. Yet given the indirect evidence for NO accumulation in our experiments, it may well be that preferential chemisorption/complexation of “heavy” intermediate NO occurs, which may lead to transient ^{15}N-depletion in the reactant NO_2^- pool. Considering that the N_2O concentrations measured in our experiments were comparatively low and that $\delta^{15}N^{bulk}$-N_2O values did not noticeably change throughout the experiments, it is unlikely that N_2O is the final product, and formation of N_2 via abiotic interactions between NO_2^- and NO is probably also involved (Doane, 2017; Phillips et al., 2016). Indeed, if accumulated as the final product, the $\delta^{15}N^{bulk}$-N_2O value at the end of the incubation should be ~-33‰ (according to closed-system accumulated-product Rayleigh dynamics), significantly higher than what we measured (~ -50 ±6 ‰). Hence, whether N_2O is an intermediate or parallel side product, its role in the overall reaction complicates N and O isotope mass balance dynamics in complex ways.

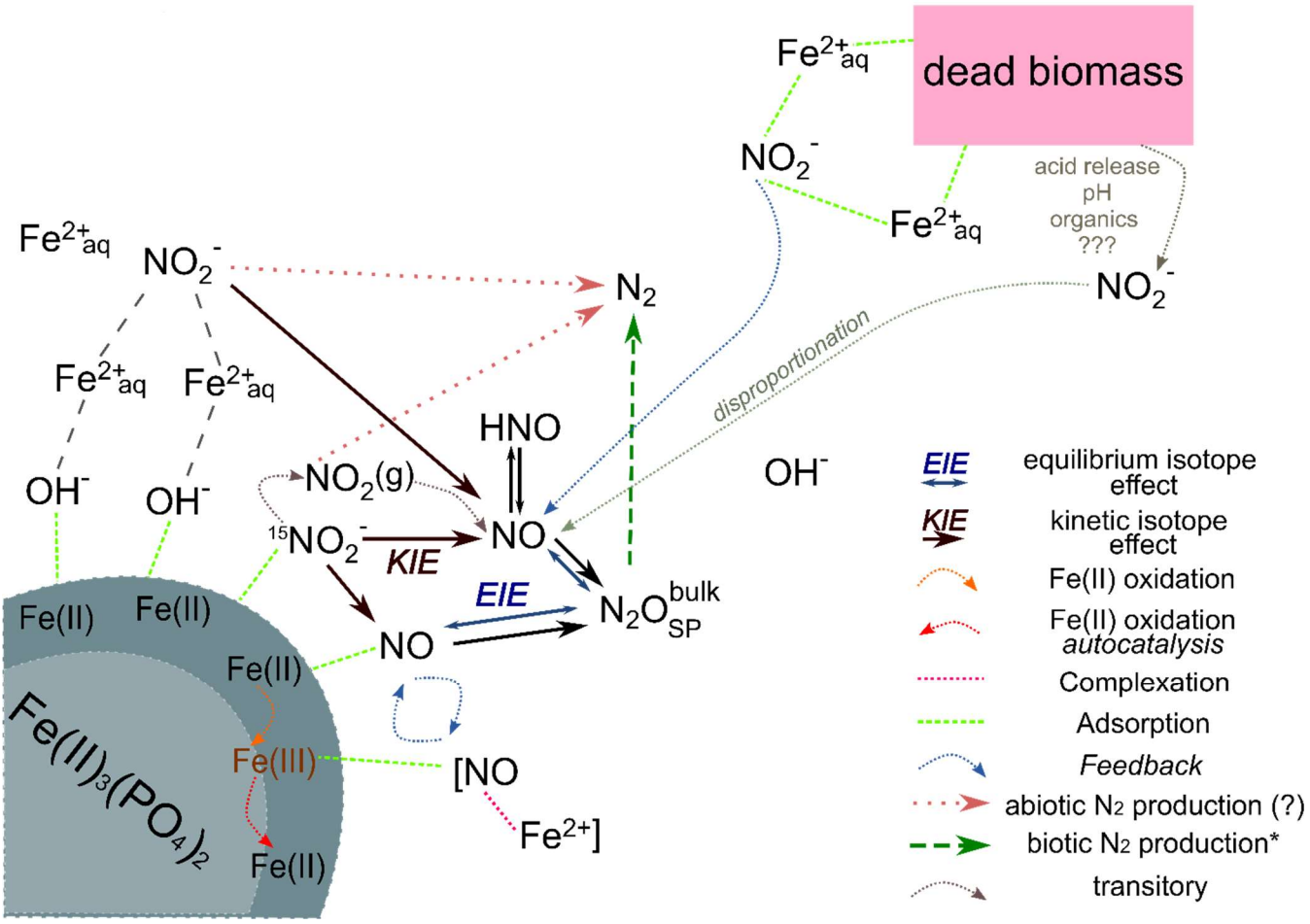

Figure 8: Conceptual figure depicting the proposed reaction mechanisms and feedbacks between the different N species during chemodenitrification induced by the presence of a mineral surface (lower left corner) or (dead) biomass (upper right corner). Adsorption of Fe^{2+} (directly or via complexation by OH^-) as well as NO_2^- could catalyse a direct reaction between both. In addition, NO_2^- adsorption onto the Fe(II) mineral might also induce disproportionation, leading to NO_x formation. These formed intermediates, although transitory, may impact the overall reaction dynamics by e.g. complex formation (i.e. [NO--Fe^{2+}]) or direct Fe(II) oxidation. The produced Fe(III) might induce another feedback loop (autocatalysis) resulting in further Fe(II) oxidation. Similar processes are possibly induced by the presence of (dead) biomass. Adsorption and complexation of either NO_2^- and Fe^{2+} would enhance the reaction between both. In addition, the presence of organic acids would decrease the pH locally and thereby promote and accelerate NO_2^- disproportionation and thus additionally enhance Fe(II) oxidation. Our results suggest that NO_2^- reduction results in an KIE, which should influence the isotopic composition of NO. N_2O here is an intermediate, the isotopic composition of which is mainly influenced by an EIE between NO and N_2O. The low N_2O yields as well as the N_2O isotopic results (bulk, SP) clearly suggests that N_2 is produced abiotically.

5. Conclusions and outlook

In the absence of any clear (genetic) evidence for enzymatic NDFeO from cultures (e.g. *Acidovorax* sp. strain BoFeN1), heterotrophic denitrification/NO_3^- reduction coupled to abiotic oxidation of Fe(II) with the NO_2^- has been presented as the most reasonable explanation for NDFeO. Here we investigated the second, abiotic step, clearly demonstrating that Fe-associated abiotic NO_2^- reduction can be catalysed by mineral and organic phases under environmentally relevant conditions, as found for example in soils and aquifers. Our results confirm that reactive surfaces play a major role with regards to the reaction between NO_2^- and Fe(II) and that surface-catalysed chemodenitrification appears to not only contribute to the production of the greenhouse gas N_2O in environments hosting active cycling of Fe and N, but also to an abiotic production of N_2. In order to understand the mechanistic details of Fe-coupled chemodenitrification, natural-abundance measurements of reactive-N isotope ratios may help distinguish between abiotic and biotic reactions during NDFeO. Our results, however, indicate that the potential of coupled N and O isotope measurements to determine the relative importance of Fe-induced N-transformations in natural environments is somewhat limited. Considering, for example, the apparent inverse N isotope effect in the mineral-only experiments, our studies show that the NO_2^- N vs. O isotope systematics seem to contrast distinctly between biotic and abiotic NO_2^- reduction, potentially permitting the disentanglement of the biotic versus abiotic processes. N_2O SP values seem to be less diagnostic with regards to discriminating between chemodenitrification-derived N_2O and N_2O that is produced during microbial NO_2^- reduction. Our results suggest that both the reaction between Fe(II) and reactive N species, as well as the resulting isotope effects, are dependent on the reactive surfaces available. The presence of organic material seems to enhance NO_2^- reduction and, to a lesser extent also N_2O production, leading to the enrichment in ^{15}N in the residual NO_2^-, as predicted by Rayleigh-type kinetic N isotope fractionation. In the presence of only Fe(II) minerals, NO_2^- reduction rates are significantly lower, and net N and O isotope effects are not governed by kinetic isotope fractionation only, but also by isotope equilibrium fractionation during exchange with the ambient mineral phase and/or the ambient water (in the case of O isotopes). While N_2O production was significant, the N_2O yields were below 5%, suggesting that a significant fraction of the NO_2^- reduced is at least transiently transformed to NO and possibly N_2. This transient pool of NO possibly stands in quasi-equilibrium with other intermediates (i.e. HNO, $NO_2(g)$) or complexes (i.e. Fe-NO), and may thereby impact the overall reaction kinetics as well.

We speculate that the transient accumulation of NO represents an important constraint both on overall reaction kinetics as well as on the N_2O isotopic signature (or $\Delta^{15}N$), an aspect that should be verified in future work. Such work may include the quantification of N_2 (and its N isotopic composition), which will help to assess to what extent (i) Fe-mineral surface-induced chemodenitrification leads to the formation of a transient pool of NO and is driven by the catalytically induced abiotic reaction between Fe(II) and NO_2^-, or if (ii) NO is actually the main oxidizing agent of Fe(II).

Our data revealed further complexity with regards to N and O isotope effects during Fe-coupled chemodenitrification than previously reported. We argue that its isotopic imprint depends on the substrate concentration, the presence of reactive surfaces or other catalysts, the mechanisms induced by these catalysts (e.g. surface complexation), and putatively on the intermediates as well as on the product present at the end of the experiments. The multifaceted control on coupled N and O isotope

667 systematics in reactive N species may explain the discrepancies observed between our and previous work (e.g. with regards to
668 $^{15}\varepsilon$:$^{18}\varepsilon$ ratios; Grabb et al. 2017). Clearly, one has to be realistic with regards to using NO_2^- and/or N_2O N and O isotope
669 measurements to provide constraints on the relative importance of chemodenitrification under natural conditions. Yet, at this
670 point, there is only a very limited number of studies on the isotope effects of chemodenitrification, and with the results
671 presented here, we expand the body of work that aims at using stable isotope measurements to assess the occurrence of
672 chemodenitrification in denitrifying environments. More work on the controls of stable isotope systematics of
673 chemodenitrification, in particular on the role of reactive, and potentially cryptic, intermediate N species, and of O isotope
674 exchange, will improve our ability to more quantitatively trace Fe-coupled nitrite reduction and N_2O production in natural Fe-
675 rich soil or sedimentary environments.

676 **Data availability**

677 Data can be accessed upon request to the corresponding author.

678 **Author contributions**

679 AAK initiated the project. MFL and AAK supervised the project. ANV designed and conducted all experiments. Isotope
680 measurements as well as data analysis were performed by ANV under the supervision of MFL. JMB conducted Mössbauer
681 measurements and data analysis. PAN supervised and performed all N_2O concentration determination measurements. ANV,
682 SDW and MFL interpreted the data and prepared the paper with inputs from all other co-authors.

683 **Competing interests**

684 The authors declare that they have no conflict of interest.

685 **Acknowledgements**

686 Special thanks go to Karen L. Casciotti (Stanford University) for helping with the correction of the N_2O isotope data. Thanks
687 to Cindy-Louise Lockwood and Toby Samuels for corrections and comments on earlier versions of the manuscript, and to
688 Viola Warter, Elizabeth Tomaszewski for fruitful discussions on abiotic chemistry and mineral reactions. Markus Maisch is
689 thanked for his help with the preparation of the Mössbauer samples and Louis Rees for his help with cultivating *S. oneidensis*
690 MR-1.

Funding

This research was supported by the Deutsche Forschungsgemeinschaft - DFG (Grants GRK 1708 Molecular principles of bacterial survival strategies), and through funds from the University of Basel, Switzerland.

References

Anderson, I. C. and Levine, J. S.: Relative Rates of Nitric Oxide and Nitrous Oxide Production by Nitrifiers, Denitrifiers, and Nitrate Respirers, Appl. Environ. Microbiol., 51(5), 938–945, 1986.

Andrews, S. C., Robinson, A. K., Rodriguez-Quinones, F. and Rodríguez-Quiñones, F.: Bacterial iron homeostasis, FEMS Microbiol. Rev., 27(2–3), 215–237, doi:10.1016/s0168-6445(03)00055-x, 2003.

Baumgärtner, M. and Conrad, R.: Role of nitrate and nitrite for production and consumption of nitric oxide during denitrification in soil, FEMS Microbiol. Lett., 101(1), 59–65, doi:10.1111/j.1574-6968.1992.tb05762.x, 1992.

Braun, V. and Hantke, K.: The Tricky Ways Bacteria Cope with Iron Limitation, pp. 31–66, Springer, Dordrecht., 2013.

Buchwald, C. and Casciotti, K. L.: Isotopic ratios of nitrite as tracers of the sources and age of oceanic nitrite, Nat. Geosci., 6(4), 308–313, doi:10.1038/ngeo1745, 2013.

Buchwald, C., Grabb, K., Hansel, C. M. and Wankel, S. D.: Constraining the role of iron in environmental nitrogen transformations: Dual stable isotope systematics of abiotic NO_2^- reduction by Fe(II) and its production of N_2O, Geochim. Cosmochim. Acta, 186, 1–12, doi:http://dx.doi.org/10.1016/j.gca.2016.04.041, 2016.

Casciotti, K. L.: Inverse kinetic isotope fractionation during bacterial nitrite oxidation, Geochim. Cosmochim. Acta, 73(7), 2061–2076, doi:10.1016/j.gca.2008.12.022, 2009.

Casciotti, K. L. and McIlvin, M. R.: Isotopic analyses of nitrate and nitrite from reference mixtures and application to Eastern Tropical North Pacific waters, Mar. Chem., 107(2), 184–201, doi:10.1016/j.marchem.2007.06.021, 2007.

Casciotti, K. L., Boehlke, J. K., McIlvin, M. R., Mroczkowski, S. J., Hannon, J. E.: Oxygen isotopes in nitrite: Analysis, calibration, and equilibration, Anal. Chem., 79(6), 2427–2436, doi:10.1021/ac061598h, 2007.

Chakraborty, A., Roden, E. E., Schieber, J. and Picardal, F.: Enhanced growth of *Acidovorax* sp. strain 2AN during nitrate-dependent Fe(II) oxidation in batch and continuous-flow systems., Appl. Environ. Microbiol., 77(24), 8548–56, doi:10.1128/AEM.06214-11, 2011.

Charlet, L., Wersin, P. and Stumm, W.: Surface charge of $MnCO_3$ and $FeCO_3$, Geochim. Cosmochim. Acta, 54(8), 2329–2336, doi:10.1016/0016-7037(90)90059-T, 1990.

Chen, D., Liu, T., Li, X., Li, F., Luo, X., Wu, Y. and Wang, Y.: Biological and chemical processes of microbially mediated nitrate-reducing Fe(II) oxidation by *Pseudogulbenkiania* sp. strain 2002, Chem. Geol., 476, 59–69, doi:10.1016/j.chemgeo.2017.11.004, 2018.

Choi, P. S., Naal, Z., Moore, C., Casado-Rivera, E., Abruna, H. D., Helmann, J. D. and Shapleigh, J. P.: Assessing the Impact of Denitrifier-Produced NO on other bacteria, Appl. Environ. Microbiol., 72(3), 2200–2205, doi:10.1128/aem.72.3.2200-2205.2006, 2006.

Van Cleemput, O. and Samater, A.: Nitrite in soils: accumulation and role in the formation of gaseous N compounds, Fertil. Res., 45(1), 81–89, doi:10.1007/BF00749884, 1995.

Coby, A. J. and Picardal, F. W.: Inhibition of NO_3^- and NO_2^- reduction by microbial Fe(III) reduction: Evidence of a reaction between NO_2^- and cell surface-bound Fe^{2+}, Appl. Environ. Microbiol., 71(9), 5267–5274, doi:10.1128/aem.71.9.5267-5274.2005, 2005.

Cornell, R. M. and Schwertmann, U.: The Iron Oxides: Structure, Properties, Reactions, Occurences and Uses, 2nd ed., Wiley-VCH., 2003.

Dai, Y.-F., Xiao, Y., Zhang, E.-H., Liu, L.-D., Qiu, L., You, L.-X., Dummi Mahadevan, G., Chen, B.-L. and Zhao, F.: Effective methods for extracting extracellular polymeric substances from *Shewanella oneidensis* MR-1, Water Sci. Technol., 74(12), 2987–2996, doi:10.2166/wst.2016.473, 2016.

Delahay, P., Pourbaix, M. and Rysselberghe, P. Van: Potential-pH diagrams, J. Chem. Educ. [online] Available from: https://pubs.acs.org/doi/pdfplus/10.1021/ed027p683 (Accessed 20 April 2018), 1950.

Dhakal, P.: Abiotic nitrate and nitrite reactivity with iron oxide minerals, University of Kentucky. [online] Available from: https://uknowledge.uky.edu/pss_etds/30, 2013.

Dhakal, P., Matocha, C. J., Huggins, F. E. and Vandiviere, M. M.: Nitrite Reactivity with Magnetite, Environ. Sci. Technol., 47(12), 6206–6213, doi:10.1021/es304011w, 2013.

Doane, T. A.: The Abiotic Nitrogen Cycle, ACS Earth Sp. Chem., 1(7), 411–421, doi:10.1021/acsearthspacechem.7b00059, 2017.

Elsner, M.: Stable isotope fractionation to investigate natural transformation mechanisms of organic contaminants: principles, prospects and limitations, J. Environ. Monit., 12(11), 2005–2031, doi:10.1039/c0em00277a, 2010.

Elsner, M., Schwarzenbach, R. P. and Haderlein, S. B.: Reactivity of Fe(II)-Bearing Minerals toward Reductive Transformation of Organic Contaminants, Environ. Sci. Technol., 38(3), 799–807, doi:10.1021/es0345569, 2004.

Expert, D.: Iron, an Element Essential to Life, in Molecular Aspects of Iron Metabolism in Pathogenic and Symbiotic Plant-Microbe Associations, pp. 1–6, Springer, Dordrecht., 2012.

Fowle, D. A. and Konhauser, K. O.: Microbial Surface Reactivity, pp. 614–616, Springer, Dordrecht., 2011.

Frame, C. H. and Casciotti, K. L.: Biogeochemical controls and isotopic signatures of nitrous oxide production by a marine ammonia-oxidizing bacterium, Biogeosciences, 7(9), 2695–2709, doi:10.5194/bg-7-2695-2010, 2010.

Fry, B.: Stable Isotope Ecology, 3rd ed., Springer Science+Business Media, LLC, New York., 2006.

Goretski, J. and Hollocher, T. C.: Trapping of nitric oxide produced during denitrification by extracellular hemoglobin, J. Biol. Chem., 263(5), 2316–2323 [online] Available from: http://www.jbc.org/content/263/5/2316.abstract, 1988.

754 Gorski, C. A. and Scherer, M. M.: Fe^{2+} sorption at the Fe oxide-water interface: A revised conceptual framework, in Aquatic
755 Redox Chemistry, vol. 1071, edited by P. G. Tratnyek, T. J. Grundl, and S. B. Haderlein, pp. 315–343, ACS
756 Publications., 2011.
757 Grabb, K. C., Buchwald, C., Hansel, C. M. and Wankel, S. D.: A dual nitrite isotopic investigation of chemodenitrification by
758 mineral-associated Fe(II) and its production of nitrous oxide, Geochim. Cosmochim. Acta, 196, 388–402 [online]
759 Available from: https://www.sciencedirect.com/science/article/pii/S0016703716306044 (Accessed 28 March 2019),
760 2017.
761 Granger, J. and Sigman, D. M.: Removal of nitrite with sulfamic acid for nitrate N and O isotope analysis with the denitrifier
762 method, Rapid Commun. Mass Spectrom., 23(23), 3753–3762, doi:10.1002/rcm.4307, 2009.
763 Granger, J., Sigman, D. M., Lehmann, M. F. and Tortell, P. D.: Nitrogen and oxygen isotope fractionation during dissimilatory
764 nitrate reduction by denitrifying bacteria, Limnol. Oceanogr., 53(6), 2533–2545, doi:10.4319/lo.2008.53.6.2533,
765 2008.
766 Granger, J., Karsh, K. L., Guo, W., Sigman, D. M. and Kritee, K.: The nitrogen and oxygen isotope composition of nitrate in
767 the environment: The systematics of biological nitrate reduction, Geochim. Cosmochim. Acta, 73(13), A460–A460,
768 2009.
769 Halder, S., Yadav, K. K., Sarkar, R., Mukherjee, S., Saha, P., Haldar, S., Karmakar, S. and Sen, T.: Alteration of Zeta potential
770 and membrane permeability in bacteria: a study with cationic agents., Springerplus, 4, 672, doi:10.1186/s40064-015-
771 1476-7, 2015.
772 He, H., Zhang, S., Zhu, C. and Liu, Y.: Equilibrium and kinetic Si isotope fractionation factors and their implications for Si
773 isotope distributions in the Earth's surface environments, Acta Geochim., 35(1), 15–24, doi:10.1007/s11631-015-
774 0079-x, 2016a.
775 He, S., Tominski, C., Kappler, A. A., Behrens, S. and Roden, E. E.: Metagenomic analyses of the autotrophic Fe(II)-oxidizing,
776 nitrate-reducing enrichment culture KS, Appl. Environ. Microbiol., 82(9), 2656–2668, doi:10.1128/AEM.03493-15,
777 2016b.
778 Heidelberg, J. F., Paulsen, I. T., Nelson, K. E., Gaidos, E. J., Nelson, W. C., Read, T. D., Eisen, J. A., Seshadri, R., Ward, N.,
779 Methe, B., Clayton, R. A., Meyer, T., Tsapin, A., Scott, J., Beanan, M., Brinkac, L., Daugherty, S., DeBoy, R. T.,
780 Dodson, R. J., Durkin, A. S., Haft, D. H., Kolonay, J. F., Madupu, R., Peterson, J. D., Umayam, L. A., White, O.,
781 Wolf, A. M., Vamathevan, J., Weidman, J., Impraim, M., Lee, K., Berry, K., Lee, C., Mueller, J., Khouri, H., Gill, J.,
782 Utterback, T. R., McDonald, L. A., Feldblyum, T. V., Smith, H. O., Venter, J. C., Nealson, K. H. and Fraser, C. M.:
783 Genome sequence of the dissimilatory metal ion–reducing bacterium Shewanella oneidensis, Nat. Biotechnol.,
784 20(11), 1118–1123, doi:10.1038/nbt749, 2002.
785 Heil, J., Vereecken, H. and Brüggemann, N.: A review of chemical reactions of nitrification intermediates and their role in
786 nitrogen cycling and nitrogen trace gas formation in soil, Eur. J. Soil Sci., 67(1), 23–39, doi:10.1111/ejss.12306,
787 2016.

Hunkeler, D. and Elsner, M.: Principles and Mechanisms of Isotope Fractionation, in Environmental Isotopes in Biodegradation and Bioremediation, edited by Aelion, C.M., Höhener, P., Hunkeler, D., and Aravena, R., pp. 43–76, CRC Press., 2009.

Ilbert, M. and Bonnefoy, V.: Insight into the evolution of the iron oxidation pathways, Biochim. Biophys. Acta - Bioenerg., 1827(2), 161–175, doi:http://dx.doi.org/10.1016/j.bbabio.2012.10.001, 2013.

Jamieson, J., Prommer, H., Kaksonen, A. H., Sun, J., Siade, A. J., Yusov, A. and Bostick, B.: Identifying and Quantifying the Intermediate Processes during Nitrate-Dependent Iron(II) Oxidation, Environ. Sci. Technol., acs.est.8b01122, doi:10.1021/acs.est.8b01122, 2018.

Jones, L. C., Peters, B., Lezama Pacheco, J. S., Casciotti, K. L. and Fendorf, S.: Stable Isotopes and Iron Oxide Mineral Products as Markers of Chemodenitrification, Environ. Sci. Technol., 49(6), 3444–3452, doi:10.1021/es504862x, 2015.

Kampschreur, M. J., Kleerebezem, R., de Vet, W. and van Loosdrecht, M.: Reduced iron induced nitric oxide and nitrous oxide emission, Water Res., 45(18), 5945–5952, doi:http://dx.doi.org/10.1016/j.watres.2011.08.056, 2011.

Kendall, C. and Aravena, R.: Nitrate Isotopes in Groundwater Systems, Environmental Tracers in Subsurface Hydrology, 261–297, doi:10.1007/978-1-4615-4557-6_9, 2000.

Klueglein, N. and Kappler, A. A.: Abiotic oxidation of Fe(II) by reactive nitrogen species in cultures of the nitrate-reducing Fe(II) oxidizer Acidovorax sp BoFeN1 - questioning the existence of enzymatic Fe(II) oxidation, Geobiology, 11(2), 396, doi:10.1111/gbi.12040, 2013.

Klueglein, N., Zeitvogel, F., Stierhof, Y.-D., Floetenmeyer, M., Konhauser, K. O., Kappler, A. A. and Obst, M.: Potential Role of Nitrite for Abiotic Fe(II) Oxidation and Cell Encrustation during Nitrate Reduction by Denitrifying Bacteria, Appl. Environ. Microbiol., 80(3), 1051–1061, doi:10.1128/aem.03277-13, 2014.

Lagarec, K. and Rancourt, D. G.: Extended Voigt-based analytic lineshape method for determining N-dimensional correlated hyperfine parameter distributions in Mössbauer spectroscopy, Nucl. Instruments Methods Phys. Res. Sect. B Beam Interact. with Mater. Atoms, 129(2), 266–280, doi:10.1016/S0168-583X(97)00284-X, 1997.

Laufer, K., Røy, H., Jørgensen, B. B. and Kappler, A. A.: Evidence for the existence of autotrophic nitrate-reducing Fe(II)-oxidizing bacteria in marine coastal sediment, Appl. Environ. Microbiol., 82(20), 6120–6131, doi:10.1128/AEM.01570-16, 2016.

Li, W., Beard, B. L. and Johnson, C. M.: Exchange and fractionation of Mg isotopes between epsomite and saturated $MgSO_4$ solution, Geochim. Cosmochim. Acta, 75, 1814–1828, doi:10.1016/j.gca.2011.01.023, 2011.

Lies, D. P., Hernandez, M. E., Kappler, A. A., Mielke, R. E., Gralnick, J. A. and Newman, D. K.: *Shewanella oneidensis* MR-1 uses overlapping pathways for iron reduction at a distance and by direct contact under conditions relevant for biofilms, Appl. Environ. Microbiol., 71(8), 4414–4426, doi:10.1128/aem.71.8.4414-4426.2005, 2005.

Liu, J. and Konermann, L.: Irreversible Thermal Denaturation of cytochrome-c studied by Electrospray Mass Spectrometry, J. Am. Soc. Mass Spectrom., 20(5), 819–828, doi:10.1016/J.JASMS.2008.12.016, 2009.

Liu, J., Wang, Z., Belchik, S. M., Edwards, M. J., Liu, C., Kennedy, D. W., Merkley, E. D., Lipton, M. S., Butt, J. N., Richardson, D. J., Zachara, J. M., Fredrickson, J. K., Rosso, K. M. and Shi, L.: Identification and Characterization of MtoA: A Decaheme c-Type Cytochrome of the Neutrophilic Fe(II)-Oxidizing Bacterium *Sideroxydans lithotrophicus* ES-1., Front. Microbiol., 3, 37, doi:10.3389/fmicb.2012.00037, 2012.

Liu, T., Chen, D., Luo, X., Li, X. and Li, F.: Microbially mediated nitrate-reducing Fe(II) oxidation: Quantification of chemodenitrification and biological reactions, Geochim. Cosmochim. Acta, doi:10.1016/J.GCA.2018.06.040, 2018.

Lovley, D. R.: Microbial Fe(III) reduction in subsurface environments, FEMS Microbiol. Rev., 20(3–4), 305–313, doi:10.1111/j.1574-6976.1997.tb00316.x, 1997.

Lovley, D. R.: Electromicrobiology, Annu. Rev. Microbiol., 66(1), 391–409, doi:10.1146/annurev-micro-092611-150104, 2012.

Luan, F., Liu, Y., Griffin, A. M., Gorski, C. A. and Burgos, W. D.: Iron(III)-Bearing Clay Minerals Enhance Bioreduction of Nitrobenzene by *Shewanella putrefaciens* CN32, Env. Sci Technol, 49, 1418–1476, doi:10.1021/es504149y, 2015.

Luna-Zaragoza, D., Romero-Guzmán, E. T. and Reyes-Gutiérrez, L. R.: Surface and Physicochemical Characterization of Phosphates Vivianite and Hydroxyapatite, J. Miner. Mater. Charact. Eng., 08(08), 591–609, doi:10.4236/jmmce.2009.88052, 2009.

Mariotti, A., Germon, J. C., Hubert, P., Kaiser, P., Letolle, R., Tardieux, A. and Tardieux, P.: Experimental determination of nitrogen kinetic isotope fractionation: Some principles; illustration for the denitrification and nitrification processes, Plant Soil, 62(3), 413–430, doi:10.1007/BF02374138, 1981.

Martin, T. S. and Casciotti, K. L.: Paired N and O isotopic analysis of nitrate and nitrite in the Arabian Sea oxygen deficient zone, Deep. Res. Part I Oceanogr. Res. Pap., 121, 121–131, doi:10.1016/j.dsr.2017.01.002, 2017.

McIlvin, M. R. and Altabet, M. A.: Chemical conversion of nitrate and nitrite to nitrous oxide for nitrogen and oxygen isotopic analysis in freshwater and seawater, Anal. Chem., 77(17), 5589–5595, doi:10.1021/ac050528s, 2005.

McIlvin, M. R. and Casciotti, K. L.: Fully automated system for stable isotopic analyses of dissolved nitrous oxide at natural abundance levels, Limnol. Oceanogr. Methods, 8(2), 54–66, doi:10.4319/lom.2010.8.54, 2010.

McKnight, G. M., Smith, L. M., Drummond, R. S., Duncan, C. W., Golden, M. and Benjamin, N.: Chemical synthesis of nitric oxide in the stomach from dietary nitrate in humans., Gut, 40(2), 211–4 [online] Available from: http://www.ncbi.nlm.nih.gov/pubmed/9071933 (Accessed 18 March 2018), 1997.

Minguzzi, A., Fan, F.-R. F., Vertova, A., Rondinini, S. and Bard, A. J.: Dynamic potential–pH diagrams application to electrocatalysts for wateroxidation, Chem. Sci., 3(1), 217–229, doi:10.1039/C1SC00516B, 2012.

Mohn, J., Wolf, B., Toyoda, S., Lin, C.-T., Liang, M.-C., Brüggemann, N., Wissel, H., Steiker, A. E., Dyckmans, J., Szwec, L., Ostrom, N. E., Casciotti, K. L., Forbes, M., Giesemann, A., Well, R., Doucett, R. R., Yarnes, C. T., Ridley, A. R., Kaiser, J. and Yoshida, N.: Interlaboratory assessment of nitrous oxide isotopomer analysis by isotope ratio mass spectrometry and laser spectroscopy: current status and perspectives, Rapid Commun. Mass Spectrom., 28(18), 1995–2007, doi:10.1002/rcm.6982, 2014.

Muehe, E. M., Gerhardt, S., Schink, B. and Kappler, A.: Ecophysiology and the energetic benefit of mixotrophic Fe(II) oxidation by various strains of nitrate-reducing bacteria, FEMS Microbiol. Ecol., 70(3), 335–343, doi:10.1111/j.1574-6941.2009.00755.x, 2009.

Muehe, E. M., Obst, M., Hitchcock, A., Tyliszczak, T., Behrens, S., Schröder, C., Byrne, J. M., Michel, F. M., Krämer, U. and Kappler, A. A.: Fate of Cd during microbial Fe(III) mineral reduction by a novel and Cd-tolerant geobacter species, Environ. Sci. Technol., 47(24), 14099–14109, doi:10.1021/es403365w, 2013.

Nelson, D. W. and Bremner, J. M.: Factors affecting chemical transformations of nitrite in soils, Soil Biol. Biochem., 1(3), 229–239, doi:10.1016/0038-0717(69)90023-6, 1969.

Niklaus, P. A., Le Roux, X., Poly, F., Buchmann, N., Scherer-Lorenzen, M., Weigelt, A. and Barnard, R. L.: Plant species diversity affects soil–atmosphere fluxes of methane and nitrous oxide, Oecologia, 181(3), 919–930, doi:10.1007/s00442-016-3611-8, 2016.

Nordhoff, M., Tominski, C., Halama, M., Byrne, J. M., Obst, M., Kleindienst, S., Behrens, S. and Kappler, A. A.: Insights into nitrate-reducing Fe(II) oxidation mechanisms through analysis of cell-mineral associations, cell encrustation, and mineralogy in the chemolithoautotrophic enrichment culture KS, Appl. Environ. Microbiol., 83(13), e00752-17, doi:10.1128/AEM.00752-17, 2017.

Ostrom, N. E. and Ostrom, P.: Handbook of Environmental Isotope Geochemistry, 1st ed., edited by M. Baskaran, Springer Berlin Heidelberg, Berlin, Heidelberg., 2011.

Ostrom, N. E. and Ostrom, P. H.: The Isotopomers of Nitrous Oxide: Analytical Considerations and Application to Resolution of Microbial Production Pathways, in Handbook of Environmental Isotope Geochemistry: Vol I, edited by M. Baskaran, pp. 453–476, Springer Berlin Heidelberg, Berlin, Heidelberg., 2012.

Ostrom, N. E., Pitt, A., Sutka, R., Ostrom, P. H., Grandy, A. S., Huizinga, K. M. and Robertson, G. P.: Isotopologue effects during N2O reduction in soils and in pure cultures of denitrifiers, J. Geophys. Res., 112(G2), doi:10.1029/2006jg000287, 2007.

Ostrom, N. E., Gandhi, H., Coplen, T. B., Toyoda, S., Böhlke, J. K., Brand, W. A., Casciotti, K. L., Dyckmans, J., Giesemann, A., Mohn, J., Well, R., Yu, L. and Yoshida, N.: Preliminary assessment of stable nitrogen and oxygen isotopic composition of USGS51 and USGS52 nitrous oxide reference gases and perspectives on calibration needs, Rapid Commun. Mass Spectrom., 32(15), 1207–1214, doi:10.1002/rcm.8157, 2018.

Otte, J. M., Blackwell, N., Ruser, R., Kappler, A. A., Kleindienst, S. and Schmidt, C.: N_2O formation by nitrite-induced (chemo)denitrification in coastal marine sediment, Sci. Rep., 9(1), 10691, doi:10.1038/s41598-019-47172-x, 2019.

Ottley, C. J., Davison, W. and Edmunds, W. M.: Chemical catalysis of nitrate reduction by iron(II), Geochim. Cosmochim. Acta, 61(9), 1819–1828, doi:Doi 10.1016/S0016-7037(97)00058-6, 1997.

Pereira, C., Ferreira, N. R., Rocha, B. S., Barbosa, R. M. and Laranjinha, J.: The redox interplay between nitrite and nitric oxide: From the gut to the brain, Redox Biol., 1(1), 276–284, doi:http://dx.doi.org/10.1016/j.redox.2013.04.004, 2013.

Phillips, R. L., Song, B., McMillan, A. M. S., Grelet, G., Weir, B. S., Palmada, T. and Tobias, C.: Chemical formation of hybrid di-nitrogen calls fungal codenitrification into question, Sci. Rep., 6(1), 39077, doi:10.1038/srep39077, 2016.

Piasecki, W., Szymanek, K. and Charmas, R.: Fe^{2+} adsorption on iron oxide: the importance of the redox potential of the adsorption system, Adsorption, doi:10.1007/s10450-019-00054-0, 2019.

Piepenbrock, A., Dippon, U., Porsch, K., Appel, E. and Kappler, A. A.: Dependence of microbial magnetite formation on humic substance and ferrihydrite concentrations, Geochim. Cosmochim. Acta, 75(22), 6844–6858, doi:10.1016/j.gca.2011.09.007, 2011.

Price, A., Macey, M. C., Miot, J. and Olsson-Francis, K.: Draft Genome Sequences of the Nitrate-Dependent Iron-Oxidizing Proteobacteria *Acidovorax* sp. Strain BoFeN1 and *Paracoccus pantotrophus* Strain KS1, edited by J. C. Thrash, Microbiol. Resour. Announc., 7(10), e01050-18, doi:10.1128/mra.01050-18, 2018.

Rakshit, S., Matocha, C. J. and Coyne, M. S.: Nitrite reduction by siderite, Soil Sci. Soc. Am. J., 72(4), 1070–1077, doi:10.2136/sssaj2007.0296, 2008.

Rancourt, D. G. and Ping, J. Y.: Voigt-based methods for arbitrary-shape static hyperfine parameter distributions in Mössbauer spectroscopy, Nucl. Instruments Methods Phys. Res. Sect. B Beam Interact. with Mater. Atoms, 58(1), 85–97, doi:10.1016/0168-583X(91)95681-3, 1991.

Rivallan, M., Ricchiardi, G., Bordiga, S. and Zecchina, A.: Adsorption and reactivity of nitrogen oxides (NO_2, NO, N_2O) on Fe-zeolites, J. Catal., 264(2), 104–116, doi:10.1016/j.jcat.2009.03.012, 2009.

Samarkin, V. A., Madigan, M. T., Bowles, M. W., Casciotti, K. L., Priscu, J. C., McKay, C. P. and Joye, S. B.: Abiotic nitrous oxide emission from the hypersaline Don Juan Pond in Antarctica, Nat. Geosci., 3(5), 341–344, doi:10.1038/ngeo847, 2010.

Schaefer, M. V.: Spectroscopic evidence for interfacial Fe(II)- Fe(III) electron transfer in clay minerals, Iowa Research Online. [online] Available from: http://ir.uiowa.edu/etd/596 (Accessed 20 March 2018), 2010.

Sigman, D. M., DiFiore, P. J., Hain, M. P., Deutsch, C., Wang, Y., Karl, D. M., Knapp, A. N., Lehmann, M. F. and Pantoja, S.: The dual isotopes of deep nitrate as a constraint on the cycle and budget of oceanic fixed nitrogen, Deep. Res. Part I-Oceanographic Res. Pap., 56(9), 1419–1439, doi:10.1016/j.dsr.2009.04.007, 2009.

Snyder, L. R. and Adler, H. J.: Dispersion in Segmented Flow through Glass Tubing in Continuous-Flow Analysis: The Ideal Model, Anal. Chem., 48(7), 1017–1022, doi:10.1021/ac60371a013, 1976.

Sorensen, J. and Thorling, L.: Stimulation by Lepidocrocite (Gamma-Feooh) of Fe(II)-Dependent Nitrite Reduction, Geochim. Cosmochim. Acta, 55(5), 1289–1294, doi:Doi 10.1016/0016-7037(91)90307-Q, 1991.

Stevenson, F. J., Harrison, R. M., Wetselaar, R. and Leeper, R. A.: Nitrosation of Soil Organic Matter: III. Nature of Gases Produced by Reaction of Nitrite with Lignins, Humic Substances, and Phenolic Constituents Under Neutral and Slightly Acidic Conditions1, Soil Sci. Soc. Am. J., 34(3), 430, doi:10.2136/sssaj1970.03615995003400030024x, 1970.

Stookey, L. L.: Ferrozine - A new spectrophotometric reagent for iron, Anal. Chem., 42(7), 779-, doi:10.1021/ac60289a016, 1970.

Straub, K. L., Benz, M., Schink, B. and Widdel, F.: Anaerobic, nitrate-dependent microbial oxidation of ferrous iron, Appl. Environ. Microbiol., 62(4), 1458–1460, 1996.

Stumm, W. and Sulzberger, B.: The cycling of iron in natural environments: Considerations based on laboratory studies of heterogeneous redox processes, Geochim. Cosmochim. Acta, 56(8), 3233–3257, doi:10.1016/0016-7037(92)90301-X, 1992.

Sutka, R. L., Ostrom, N. E., Ostrom, P. H., Breznak, J. A., Gandhi, H., Pitt, A. J. and Li, F.: Distinguishing nitrous oxide production from nitrification and denitrification on the basis of isotopomer abundances, Appl. Environ. Microbiol., 72(1), 638–644, doi:10.1128/Aem.72.1.638-644.2006, 2006.

Tanford, C.: Protein denaturation: Part c. theoretical models for the mechanism of denaturation, Adv. Protein Chem., 24(C), 1–95, doi:10.1016/S0065-3233(08)60241-7, 1970.

Taran, Y. A., Kliger, G. A., Cienfuegos, E. and Shuykin, A. N.: Carbon and hydrogen isotopic compositions of products of open-system catalytic hydrogenation of CO_2: Implications for abiogenic hydrocarbons in Earth's crust, Geochim. Cosmochim. Acta, 74(21), 6112–6125, doi:10.1016/j.gca.2010.08.012, 2010.

Tian, T., Zhou, K., Xuan, L., Zhang, J.-X., Li, Y.-S., Liu, D.-F. and Yu, H.-Q.: Exclusive microbially driven autotrophic iron-dependent denitrification in a reactor inoculated with activated sludge, Water Res., 170, 115300, doi:10.1016/j.watres.2019.115300, 2020.

Tiso, M. and Schechter, A. N.: Nitrate reduction to nitrite, nitric oxide and ammonia by gut bacteria under physiological conditions., PLoS One, 10(3), e0119712, doi:10.1371/journal.pone.0119712, 2015.

Tominski, C., Heyer, H., Lösekann-Behrens, T., Behrens, S. and Kappler, A. A.: Growth and Population Dynamics of the Anaerobic Fe(II)-Oxidizing and Nitrate-Reducing Enrichment Culture KS, edited by F. E. Löffler, Appl. Environ. Microbiol., 84(9), e02173-17, doi:10.1128/AEM.02173-17, 2018.

Toyoda, S. and Yoshida, N.: Determination of Nitrogen Isotopomers of Nitrous Oxide on a Modified Isotope Ratio Mass Spectrometer, , doi:10.1021/AC9904563, 1999.

Toyoda, S., Mutobe, H., Yamagishi, H., Yoshida, N. and Tanji, Y.: Fractionation of N_2O isotopomers during production by denitrifier, Soil Biol. Biochem., 37(8), 1535–1545, doi:10.1016/j.soilbio.2005.01.009, 2005.

Veeramani, H., Alessi, D. S., Suvorova, E. I., Lezama-Pacheco, J. S., Stubbs, J. E., Sharp, J. O., Dippon, U., Kappler, A. A., Bargar, J. R. and Bernier-Latmani, R.: Products of abiotic U(VI) reduction by biogenic magnetite and vivianite, Geochim. Cosmochim. Acta, 75(9), 2512–2528, doi:10.1016/j.gca.2011.02.024, 2011.

Wankel, S. D., Ziebis, W., Buchwald, C., Charoenpong, C., De Beer, Di., Dentinger, J., Xu, Z. and Zengler, K.: Evidence for fungal and chemodenitrification based N_2O flux from nitrogen impacted coastal sediments, Nat. Commun., 8(1), 15595, doi:10.1038/ncomms15595, 2017.

Weber, K. A., Hedrick, D. B., Peacock, A. D., Thrash, J. C., White, D. C., Achenbach, L. A. and Coates, J. D.: Physiological and taxonomic description of the novel autotrophic, metal oxidizing bacterium, *Pseudogulbenkiania* sp. strain 2002, Appl. Microbiol. Biotechnol., 83(3), 555–565, doi:10.1007/s00253-009-1934-7, 2009.

Well, R. and Flessa, H.: Isotopologue signatures of N_2O produced by denitrification in soils, J. Geophys. Res., 114, doi:10.1029/2008jg000804, 2009.

Wenk, C. B., Frame, C. H., Koba, K., Casciotti, K. L., Veronesi, M., Niemann, H., Schubert, C. J., Yoshida, N., Toyoda, S., Makabe, A., Zopfi, J. and Lehmann, M. F.: Differential N_2O dynamics in two oxygen-deficient lake basins revealed by stable isotope and isotopomer distributions, Limnol. Oceanogr., 61(5), 1735–1749, doi:10.1002/lno.10329, 2016.

White, G. F., Edwards, M. J., Gomez-Perez, L., Richardson, D. J., Butt, J. N. and Clarke, T. A.: Mechanisms of Bacterial Extracellular Electron Exchange, in Advances in Microbial Physiology, vol. 68, pp. 87–138., 2016.

Widdel, F. and Pfennig, N.: Studies on dissimilatory Sulfate-reducing Bacteria that decompose Fatty-Acids - 1. Isotolation of New Sulfate-reducing Bacteria enriched with Acetate from saline Environments - Description of Desulfobacter postgatei gen. nov. sp. nov., Arch. Microbiol., 129(5), 395–400, doi:10.1007/bf00406470, 1981.

Widdel, F., Kohring, G.-W. and Mayer, F.: Studies on Dissimilatory Sulfate-Reducing Bacteria that Decompose Fatty Acids, Arch Microbiol, 134, 286–294 [online] Available from: https://link.springer.com/content/pdf/10.1007/BF00407804.pdf (Accessed 22 April 2018), 1983.

Wilson, W. W., Wade, M. M., Holman, S. C. and Champlin, F. R.: Status of methods for assessing bacterial cell surface charge properties based on zeta potential measurements, J. Microbiol. Methods, 43(3), 153–164, doi:10.1016/S0167-7012(00)00224-4, 2001.

Winther, M., Balslev-Harder, D., Christensen, S., Priemé, A., Elberling, B., Crosson, E. and Blunier, T.: Continuous measurements of nitrous oxide isotopomers during incubation experiments, Biogeosciences, 15(3), 767–780, doi:10.5194/bg-15-767-2018, 2018.

Wunderlin, P., Lehmann, M. F., Siegrist, H., Tuzson, B., Joss, A., Emmenegger, L. and Mohn, J.: Isotope Signatures of N_2O in a Mixed Microbial Population System: Constraints on N_2O Producing Pathways in Wastewater Treatment, Environ. Sci. Technol., 130118101927005, doi:10.1021/es303174x, 2013.

Ye, R. W., Averill, B. A. and Tiedje, J. M.: Denitrification: production and consumption of nitric oxide, Appl. Environ. Microbiol., 60(4), 1053–1058 [online] Available from: http://www.ncbi.nlm.nih.gov/pmc/articles/PMC201439/, 1994.

Zeitvogel, F., Burkhardt, C. J., Schroeppel, B., Schmid, G., Ingino, P. and Obst, M.: Comparison of Preparation Methods of Bacterial Cell-Mineral Aggregates for SEM Imaging and Analysis Using the Model System of *Acidovorax sp.* BoFeN1, Geomicrobiol. J., 34(4), 317–327, doi:10.1080/01490451.2016.1189467, 2017.

Zhu-Barker, X., Cavazos, A. R., Ostrom, N. E., Horwath, W. R. and Glass, J. B.: The importance of abiotic reactions for nitrous oxide production, Biogeochemistry, 126(3), 251–267, doi:10.1007/s10533-015-0166-4, 2015.

989 Zumft, W. G.: Cell biology and molecular basis of denitrification, Microbiol. Mol. Biol. Rev., 61(4), [online] Available from:
990 http://www.ncbi.nlm.nih.gov/pubmed/9409151 (Accessed 19 February 2018), 1997.
991 Zweier, J. L., Samouilov, A. and Kuppusamy, P.: Non-enzymatic nitric oxide synthesis in biological systems, Biochim.
992 Biophys. Acta - Bioenerg., 1411(2–3), 250–262, doi:10.1016/S0005-2728(99)00018-3, 1999.
993